

Non-identical particle femtoscopy at $\sqrt{s_{NN}} = 200$ GeV in hydrodynamics with statistical hadronization*

Adam Kisiel^{1,2,†}

¹*Department of Physics, Ohio State University, 1040 Physics Research Building,
191 West Woodruff Ave., Columbus, OH 43210, USA*

²*Faculty of Physics, Warsaw University of Technology, PL-00661 Warsaw, Poland*

Non-identical particle femtoscopy probes not only the size of the emitting system, but also the emission asymmetries between particles of different mass, which are intimately related with the collective behavior of matter. We apply the technique to the simulations from the THERMINATOR+Lhyquid model of the heavy-ion collisions at $\sqrt{s_{NN}} = 200$ GeV. We present predictions for all pairwise combinations of pions, kaons, and protons, and discuss their interpretation. We show that kaon and proton distributions are strongly influenced by flow: the source gets smaller and shifted to the outside with growing p_T , while for pions the shift is significantly smaller, producing an emission asymmetry. We explain how particles coming from decays of hadronic resonances enhance the asymmetry signal coming from flow, contrary to naive expectations. Emphasis is put on extracting this unique information about collective behavior of matter from the non-identical particle correlations. We also present, in detail, the technical aspects of the non-identical particle femtoscopy technique applied to data from the heavy-ion collisions. We list the sources of systematic errors coming from the method itself and the usual assumptions. We describe robust analysis methods and discuss their limitations.

PACS numbers: 25.75.-q, 25.75.Dw, 25.75.Ld

Keywords: relativistic heavy-ion collisions, hydrodynamics, femtoscopy, non-identical particle correlations, RHIC, LHC

I. INTRODUCTION

Femtoscopy has been used for more than 35 years [1, 2] to measure sizes of the systems created in nucleus-nucleus collisions. Initially it was developed for analyzing the two-particle correlation arising from the wave-function symmetrization for pairs of identical particles [3] and was similar in mathematical framework to the “HBT interferometry” used in astronomy [4–6]. Later it was realized that similar correlations arise due to the Final State Interactions (Coulomb and Strong) between particles that are not necessarily identical [7–11].

Femtoscopy of non-identical particles provides unique information: while the identical particle correlation usually only measure the “size” of the emitting region (more precisely, the second moments of the emission function), non-identical correlations can, thanks to the very fact that they correlate particles that are not identical, also measure the relative emission shifts (the first moments of the emission function) [7–10, 12–14].

The unique features of the non-identical particle femtoscopy was used in low-energy nuclear collisions to study the time ordering of the emission of various nuclear fragments from the compound nucleus [15–19]. This required measuring time differences from several to hundreds of fm/c [16–19].

In this work we focus on the applications of this tech-

nique in the collisions of ultra-relativistic heavy ions, specifically Au ions at the Relativistic Heavy Ion Collider (RHIC) in Brookhaven National Laboratory (BNL), although the discussion is also relevant for lower (at Super Proton Synchrotron SPS of CERN) and higher (Large Hadron Collider LHC at CERN) energy collisions.

One of the major discoveries at RHIC has been the observation of the Quark Gluon Plasma (QGP), which was found to behave collectively, very much like a fluid [20, 21]. Hydrodynamic equations seemed to describe this behavior well in the momentum sector. However attempts to simultaneously describe the space-time behavior measured by femtoscopy have not been successful until recently. This failure was commonly referred to as the “RHIC hydro HBT puzzle” [22–25]. Through a detailed analysis of the experimental data and various improvements of the hydrodynamic description it was realized that certain assumptions had to be modified in order to properly describe both sets of observables. The initial condition was changed to the one that uses Gaussian initial profile for the transverse energy density [26], which results in faster development of the initial flow, compared the traditional one [27, 28]. The equation-of-state used did not exhibit a first-order phase transition, but rather a cross-over. The detailed simulation of the resonances contribution in the later stage of the collisions was carried out [26]. In addition, some studies suggest that the introduction of viscosity and universal (pre-equilibrium flow) into the model may also play an important role [29, 30].

The hydrodynamic scenario produces specific space-momentum correlation patterns, which are commonly referred to as flow. The system created in the heavy-ion collision expands rapidly outwards, showing a very

*Supported by the U.S. NSF Grant No. PHY-0653432.

†Electronic address: kisiel@if.pw.edu.pl

strong radial flow, which is observed in the modification of the single particle inclusive p_T spectra shape. In addition, in non-central collisions, the initial overlap region has an elongated (usually described as “almond”) shape, and this spatial asymmetry is converted to the momentum one in the final state. This momentum asymmetry is observed as an elliptic flow v_2 and is the subject of very intensive theoretical and experimental studies; see [31, 32] for recent reviews. However, because of its origin, it is small in central collisions. This is unfortunate, since it is in central collisions that we expect to create the largest volume of deconfined matter, which we would like to study. Both the p_T spectra and the elliptic flow are observables depending only on the momenta of the particles, so their connection to space-time can only be indirectly inferred. To access it directly we employ femtoscopic techniques. It is argued that the fall of the “femtoscopic radii” with particle’s m_T can be interpreted as the decrease of “lengths of homogeneity”, a direct consequence of radial and longitudinal flow [33]. However, one might come up with alternative explanations, involving temperature gradients to produce similar dependencies [34]. In this work we will show how the collective flow present in hydrodynamic and transport models, in addition to the effects discussed above, produces differences in average emission points between particles of different masses. We will also describe how these emission asymmetries can be accessed via the non-identical particle femtoscopy [35]. Measuring such effects would enable us to eliminate scenarios alternative to hydrodynamic expansion and provide a crucial and strict test for the models. Results on $\pi^+-\pi^-$ and π -proton correlations have been previously reported by NA49 [35, 36] and the CERES experiment [37, 38] at the SPS. The first results on pion-kaon correlations have been reported by STAR [39]. Preliminary results on π - Ξ correlations from STAR have also been presented [40]. Proton- Λ correlations have also been measured by STAR [41], but this analysis did not attempt to extract emission asymmetries.

In order to properly simulate the emission asymmetries between particles of different masses we need a model which has all the important features: the hydrodynamic phase which produces space-momentum correlations and the hadronic phase where at least the hadronic resonance decays and propagation is treated. In addition the model should provide the space-time freeze-out coordinates of particles, so that femtoscopic calculations can be carried out. It should, as much as possible, reproduce the available data on particle spectra and femtoscopy. Hydrodynamics inspired “blast-wave” parametrization of freeze-out have been used to model asymmetries between non-identical particles [42]. This study nicely illustrated the connection between strong collective matter behavior and the asymmetries; however it used simplified emission functions and neglected the resonance propagation and decay. In this work we have chosen the THERMINATOR+Lhyquid model, which we in-

troduce in Section II. In Section III we describe the particular set of simulations of heavy-ion collisions at six centralities that we have carried out. We calculated the system size and emission asymmetry for three pair types: pion-kaon, pion-proton and kaon-proton. We discuss the origins of the asymmetry and provide the connection to the space-momentum correlations coming from flow. We also discuss other non-flow sources of emission asymmetries and provide a quantitative estimate of all contributions.

Having emphasized the importance of the emission asymmetries phenomenon we proceed to describe the theoretical framework of the non-identical particle correlations in Section IV. Then, we move to the technical aspects of the measurement in heavy-ion collisions in Section V. We argue that a specific mathematical representation of the non-identical correlation functions (the spherical harmonics decomposition) shows remarkable synergies with the analysis and maximizes the statistical significance of the emission asymmetry signal. We describe the measurement procedure which enables to recover the properties of the model emission function from the “experimental” correlation function. In Section VI we test the robustness of the procedure, list the assumptions and the approximations that need to be employed and estimate the systematic error coming from the technique itself. We show that the most important contribution to this error is the correct estimation of the fraction of non femtoscopically correlated pairs (traditionally called “purity”). We analyze this effect in detail and present purity estimates, based on our model of choice, which can be directly used in the experimental analysis.

Finally, in Section VII we use numerical simulations with the THERMINATOR model to produce “experimental-like” correlation functions, which we then analyze with the methods presented earlier. We demonstrate that the method is able to recover the theoretical input values. The results presented in this section are the theoretical predictions for the overall system size as well as the emission asymmetry for all considered pair types and 6 centralities. They can be immediately compared to the experimental results with minimal number of approximations, and therefore minimal systematic uncertainty.

II. LHYQUID + THERMINATOR MODEL

In this work we use what we call the *standard approach*, consisting of ideal-fluid hydrodynamics followed by statistical hadronization. Numerous calculations have been performed in this framework, with the common difficulty [22] of simultaneously describing femtoscopy and other signatures in the data. More precisely, the *RHIC HBT puzzle* [22–25] refers to problems in reconciling the large value of the elliptic flow coefficient, v_2 , with the identical particle interferometry in calculations based on hydrodynamics [43–47]. Recently, a successful uniform description of soft observables at RHIC has been ac-

complished, including the femtoscopic radii, within the standard approach [26]. The essential ingredients of this analysis are the Gaussian initial condition for hydrodynamics, early start of the evolution, the state-of-the-art equation of state with smooth crossover, and the use of THERMINATOR [48] with all resonances from SHARE [49] incorporated to carry out the statistical hadronization at the freeze-out surface of temperature 150 MeV. The interplay of these elements resulted in a simultaneous description of the transverse-momentum spectra of pions, kaon and protons, the v_2 , and the femtoscopic correlation radii of pions, including full centrality, k_T and reaction plane dependence of azimuthally sensitive HBT signatures [50].

In this section we describe the essential elements of our method to the extent they are necessary for the presented new results. More details concerning the hydrodynamics can be found in Refs. [26, 51, 52], while the method used for femtoscopic calculations has been presented in Ref. [53].

A. Initial condition

As reported in Ref. [26], the use of the initial condition for hydrodynamics of the Gaussian form,

$$n(x, y) = \exp\left(-\frac{x^2}{2a^2} - \frac{y^2}{2b^2}\right), \quad (1)$$

where n is the initial energy density, while x and y denote the transverse coordinates, leads to a much better uniform description of the data for the p_T -spectra, v_2 , and the pionic femtoscopic radii compared to the use of the standard initial condition from the Glauber model.

The width parameters a and b depend on centrality. In order to estimate realistic values for them we run the GLISSANDO [54] Glauber Monte Carlo simulations which include the eccentricity fluctuations [55, 56]. Then we match a^2 and b^2 to reproduce the values $\langle x^2 \rangle$ and $\langle y^2 \rangle$ from the GLISSANDO profiles. Thus, by construction, the spatial RMS radii of the initial condition and its eccentricity is the same as the ones from the Glauber calculation. Nevertheless, the shape is not the same. The Gaussian profiles are sharper near the origin, which results in a faster buildup of the Hubble-like flow in the hydrodynamical stage.

The Glauber calculations, needed to obtain the a and b parameters, correspond to the mixed model [57], where the number of produced particles is proportional to $(1 - \alpha)N_w/2 + \alpha N_{\text{bin}}$, with N_w and N_{bin} denoting the number of wounded nucleons [58] and binary collisions, respectively. The parameter $\alpha = 0.145$ for top RHIC energy [59, 60]. The inelastic nucleon cross section is 42 mb for RHIC [61]. The simulations incorporate the fluctuations of orientation of the fireball (the variable-axes geometry), which result in increased eccentricity compared to the fixed-axes geometry [62]. Finally, the expulsion distance of 0.4 fm is used in the generation of the nuclear

distributions. A source-dispersion parameter of 0.7 fm is used. It describes the random displacement of the source from the center of the wounded nucleon or the binary-collision position [54].

The values of the a and b parameters for various centralities and the corresponding eccentricity parameters

$$\epsilon^* = \frac{b^2 - a^2}{a^2 + b^2}, \quad (2)$$

are collected in Table I.

The energy-density profile (1) determines the initial temperature profile via the equation of state [52]. The initial central temperature, T_i , is a parameter dependent on centrality. For RHIC calculations it is adjusted to reproduce the total particle multiplicity.

B. Hydrodynamics

The hydrodynamics equations used in this work were described in greater detail in Refs. [51, 52]. We use inviscid (ideal-fluid), baryon-free, boost-invariant hydrodynamics. The equations are written in terms of the velocity of sound, c_s , whose temperature dependence encodes the full information on the equation of state of the system. We incorporate the known features of $c_s(T)$, which, at high temperatures, are given by the lattice QCD calculations [63]; at low T they follow from the hadron gas including all resonances, while at intermediate T an interpolation is used. No sharp phase transition, but a smooth cross-over, is built in, in accordance to the present knowledge of the thermodynamics of QCD at zero baryon chemical potential. The plot of the resulting $c_s(T)$ can be found in Ref. [26].

The initial proper time of the start of hydrodynamics is fixed to the value

$$\tau_0 = 0.25 \text{ fm}. \quad (3)$$

This early start of hydrodynamics allows for a fast generation of transverse flow, similar to the effect described in [30].

C. Freeze-out

The hydrodynamic evolution proceeds until freeze-out occurs, where the assumed condition for the *universal* freeze-out temperature is $T_f = 150$ MeV. This value is somewhat lower than in several fits of the chemical freeze-out [64–66]; however, it agrees with the recently made global fits to particle transverse momentum spectra of Ref. [67, 68], where the value around 150 MeV was obtained for the kinetic freeze-out temperature.¹

¹ The use of this lower freeze-out temperature needs the introduction of the strangeness inequilibrium factors γ_s in order to

TABLE I: Shape parameters a and b of Eq. (1) for various centrality classes obtained by matching $\langle x^2 \rangle$ and $\langle y^2 \rangle$ to GLISSANDO simulations, the variable-axes eccentricity ϵ^* , and the central temperature T_i .

c [%]	0-5	5-10	10-20	20-30	30-40	40-50	50-60	60-70	70-80
RHIC Au+Au at $\sqrt{s_{NN}} = 200$ GeV									
a [fm]	2.70	2.54	2.38	2.00	1.77	1.58	1.40	1.22	1.04
b [fm]	2.93	2.85	2.74	2.59	2.45	2.31	2.16	2.02	1.85
ϵ^*	0.08	0.12	0.18	0.25	0.31	0.36	0.41	0.46	0.52
T_i [MeV]	500	491	476	460	429	390	344	303	261

THERMINATOR is used to carry out the statistical hadronization at the freeze-out hypersurface according to the Cooper-Frye formulation [69]. According to the assumed single-freeze-out approximation, identifying the kinetic and chemical freeze-out temperatures, rescattering processes after freeze-out are neglected. We have checked that the collision rate after freeze-out is moderate for the hypersurfaces applied in this work. We estimate it by considering a pion straight-line trajectory and counting the number of encounters with other particles closer than the distance corresponding to the pion-hadron cross section. The average number of these trajectory crossings is about 1.5-1.7 per pion. This shows that the single-freeze-out approximation [65] works reasonably well for the present case. At a more detailed level, one could use hadronic afterburners to model the elastic collisions [70–72], or attempt the hydro-kinetic approach implemented in [27, 28, 73].

D. Two-particle femtoscopy

The method used for femtoscopic analysis of the THERMINATOR model output was described in detail in Ref. [53]. The features of the formalism specific to the non-identical particle correlations are described in Section IV. Their discussion is one of the main points of this work.

III. MODEL PREDICTIONS FOR RHIC

In this section we discuss the general trends that are expected to emerge in the non-identical correlations. We also discuss their physical origins and the possible physics conclusions that can be drawn when they are observed experimentally. Later in this paper, we will see how these trends manifest themselves in the calculations and we test whether it is indeed possible to observe them in the experiment.

Following convention, we assign symbol x for the emission points of single particles, usually used as a vector,

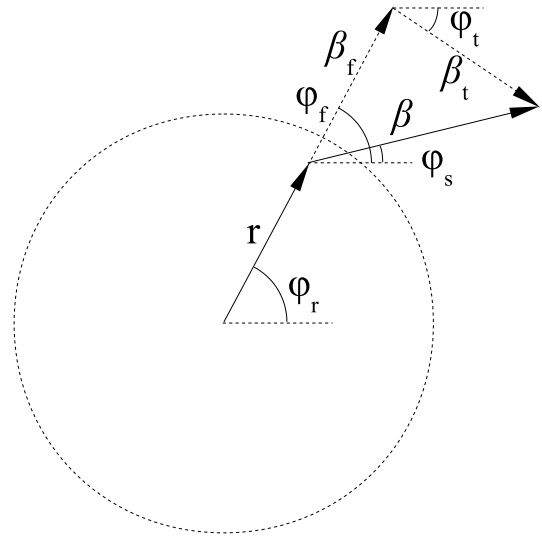


FIG. 1: Diagram of the particle's velocity β decomposition into the flow β_f and thermal β_t components.

\mathbf{x} , or as a vector magnitude, x . Momentum of a particle is denoted as p . Single particle velocity is β . We also define the pair variables. Relative separation between particles (vector) is: $\mathbf{r} = \mathbf{x}_1 - \mathbf{x}_2$. We use the out-side-long coordinate system, where the *long* or *longitudinal* direction is along the beam axis, the *out* or *outward* direction is along the pair total transverse momentum and the *side* or *sideward* is perpendicular to the other two. In Longitudinally Co-Moving System (LCMS) the pair longitudinal momentum vanishes: $p_{1,long} = -p_{2,long}$. In the Pair Rest Frame (PRF) (also called Pair Center of Mass (PCOM)) the pair center-of-mass rests: $\mathbf{p}_1 = -\mathbf{p}_2$. In our convention all pair variables in PRF are marked by an asterisk. The pair relative momentum half is denoted as k^* and is equal to the *first* particle's momentum in PRF. The pair total momentum is denoted as P (or sometimes K traditionally used in identical particle femtoscopy). All single-particle coordinates as well as pair relative variables use lower case letters. In contrast we will use upper-case letters to denote the parameters of distributions. In particular we call the variance or the two-particle separation distribution R . We call the mean of such distribution μ (with the L superscript if they are defined in LCMS). We refer the reader to Appendix A for explicit mathematical formulas as well as relations be-

reproduce the abundances of strange particles [67].

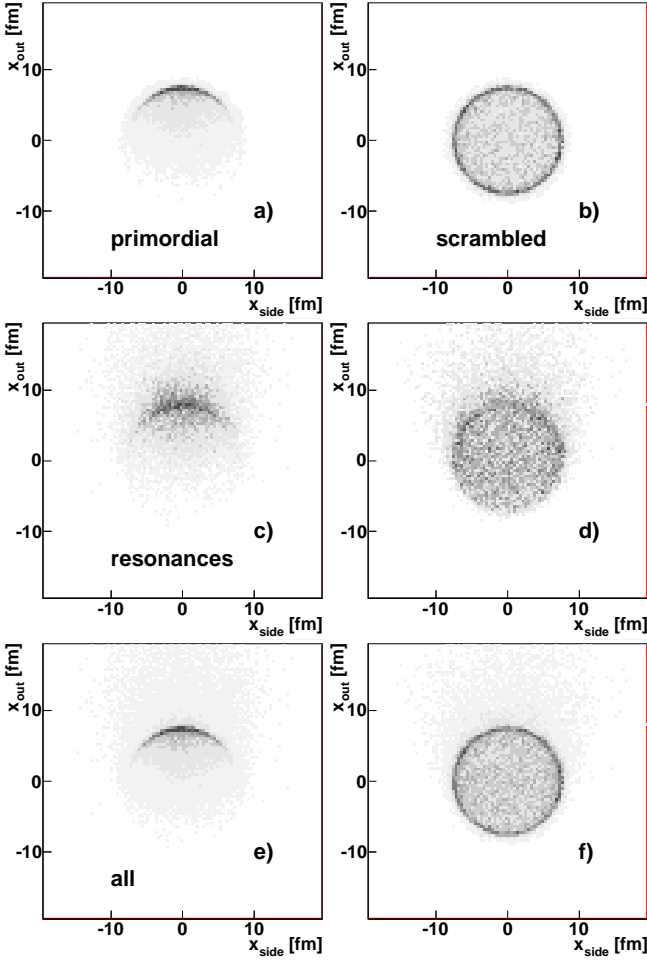


FIG. 2: Emission points of particles with the velocity in $(0.6, 0.8)$, its direction pointing “upwards”, for kaons, central Au+Au. Panels a), c), e) show standard simulation results, panels b), d), f): with flow correlation “scrambled” (see text for details). Upper plots a), b) show primordial particles, center c), d): particles coming from resonance decays, lower e), f): all.

tween source characteristics in the two reference frames.

The discussion below is based on an example calculation from the THERMINATOR+Lhyquid model, done for parameters tuned to the central (0-5%) RHIC Au+Au collisions at $\sqrt{s_{NN}} = 200$ GeV. Whenever we mention RHIC Au+Au calculations we mean simulations at the top RHIC energy.

A. Emission asymmetries

Hydrodynamic evolution of matter implies strong space-momentum correlations in particle emission. Particles emitted from a given fluid cell will have a velocity which is a combination of two components: the fluid cell velocity β_f (taken from the flow field $u_\mu(\mathbf{r})$) and the thermal velocity β_t . This is schematically shown in Fig. 1.

The system created in heavy-ion collision, when mod-

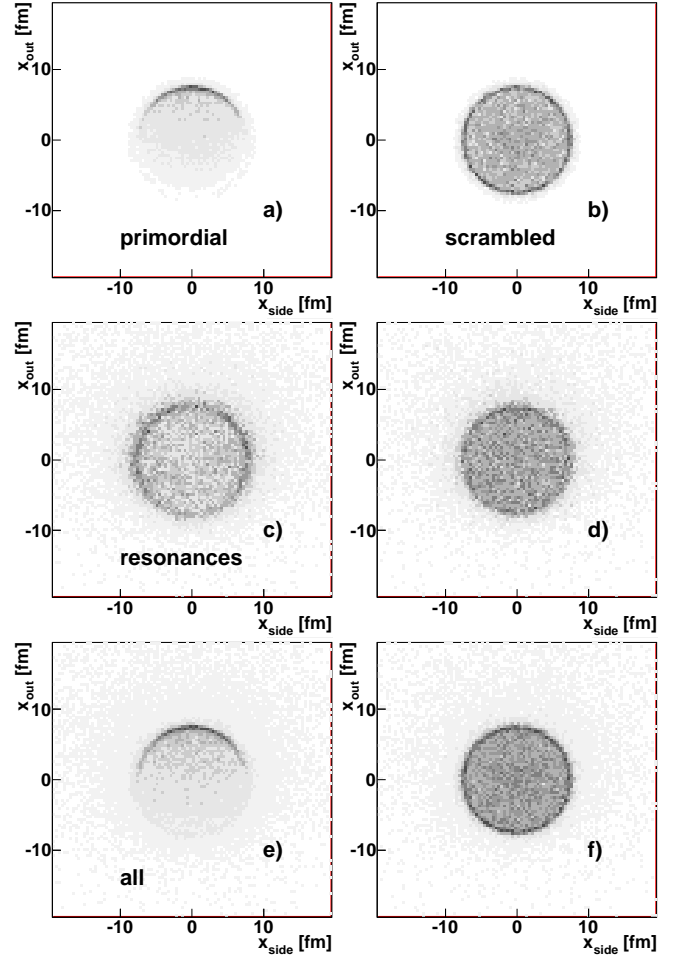


FIG. 3: Emission points of particles with the velocity magnitude in the range $(0.6, 0.8)$, its direction pointing “upwards”, for pions, central Au+Au. Panels notation the same as in Fig. 2.

eled in hydrodynamics, naturally develops a collective behavior - the radial flow in the transverse plane, that is matter is collectively moving “outwards” from the central axis of the source to the outside. In essence this is an $x-p$ correlation - the direction ϕ_f of the fluid element’s transverse velocity is aligned with it’s transverse position vector direction ϕ_r . When the fluid element emits particles, all of them will have the same common flow velocity β_f taken directly from u_μ . To this velocity one adds a thermal component β_t which has a random direction ϕ_t in the rest frame of the fluid element. It will dilute the $x-p$ directional correlation. Let us now consider the mean emission point of a single particle, more specifically its component parallel to the velocity [74]:

$$x_{out} = \frac{\mathbf{x}\beta}{\beta} = \frac{r(\beta_f + \beta_t \cos(\phi_t - \phi_f))}{\beta}. \quad (4)$$

We analyze its average over particles at fixed β . If we assume a Gaussian density profile with radius r_0 and linear transverse velocity profile $\beta_f = \beta_0 r/r_0$ then we

TABLE II: Single-particle source parameters (mean $\langle r \rangle$ and RMS X) for three particle types in selected kinematic regions.

Particle	β	p_T [GeV/c]	X_{out} [fm]	$\langle x_{out} \rangle$ [fm]	X_{side} [fm]	$\langle x_{side} \rangle$ [fm]
primordial						
K	0.6-0.8	0.42-0.56	2.68	4.46	3.25	0.03
π	0.6-0.8	0.12-0.16	3.47	2.85	3.66	-0.02
π	0.95-0.97	0.42-0.56	2.56	4.81	3.31	-0.01
p	0.6-0.8	0.80-1.06	2.02	5.40	2.82	-0.05
π	0.6-0.8	0.12-0.16	3.47	2.85	3.66	-0.02
π	0.985-0.991	0.80-1.06	1.88	5.68	2.90	0.00
all						
K	0.6-0.8	0.42-0.56	2.99	4.97	3.55	0.00
π	0.6-0.8	0.12-0.16	4.52	1.73	4.72	-0.03
π	0.95-0.97	0.42-0.56	2.94	5.03	3.20	-0.01
p	0.6-0.8	0.80-1.06	2.31	6.12	2.88	-0.02
π	0.6-0.8	0.12-0.16	4.52	1.73	4.52	-0.02
π	0.985-0.991	0.80-1.06	2.19	6.20	3.08	-0.01

TABLE III: Mean emission points and pair asymmetries for pions, kaons and protons with velocity (0.6, 0.8) in central Au+Au simulation. Averaging is done over all pairs in this range. See text for explanation of “flow” and “scrambled”.

	$\langle x_{out}^{\pi} \rangle$	$\langle x_{out}^K \rangle$	$\langle x_{out}^p \rangle$	$\langle x_{out}^{\pi} \rangle - \langle x_{out}^K \rangle$	$\langle x_{out}^{\pi} \rangle - \langle x_{out}^p \rangle$	$\langle x_{out}^K \rangle - \langle x_{out}^p \rangle$
flow						
primordial	2.83	4.47	5.61	-1.64	-2.78	-1.14
non-primordial	1.34	7.35	9.19			
all	2.00	5.54	6.69	-3.54	-4.69	-1.15
scrambled						
primordial	-0.04	0.00	-0.03	-0.04	-0.01	0.03
non-primordial	0.88	3.17	4.20			
all	0.48	1.20	1.28	-0.72	-0.80	-0.08

obtain [74]:

$$\langle x_{out} \rangle = \frac{\langle r\beta_f \rangle}{\langle \sqrt{\beta_t^2 + \beta_f^2} \rangle} = \frac{r_0\beta_0\beta}{\beta_0^2 + T/m_t}, \quad (5)$$

where we have explicitly given the formula for the velocity component coming from temperature. Pions and kaons emitted from the fluid element will have the same common flow velocity β_f (and different momenta). They will also get a random thermal kick, depending on momentum. For a pion the same p_T kick will mean much larger *velocity* β_t kick, than for a kaon. The final velocity direction of a pion will be, on average, less correlated with its emission position than that of a kaon. We assume that the spatial characteristics of pion and kaon emission are the same and the flow velocity is also the same. Hence, for both pions and kaons, $\langle r\beta_f \rangle$ is the same. The only difference is the T/m_T component, smaller for kaons. Therefore, $\langle x_{out} \rangle$ for pions is smaller than $\langle x_{out} \rangle$ for kaons. Summarizing: when correlating pions and kaons with the same velocity (or more generally two non-identical particles of different masses, but same velocity) pions (lighter particles) appear to be, on average, emitted closer to the center of

the system than kaons (heavier particles). Consequently, hydrodynamics predicts a negative emission asymmetry $\mu_{out}^{light,heavy} = \langle r_{out}^{light,heavy} \rangle = \langle x_{out}^{light} - x_{out}^{heavy} \rangle$ between non-identical particles of different masses².

Let us discuss various limits in Eq. (5). When there is no flow ($\beta_f = 0$), all average emission points are zero and the asymmetry vanishes. If the temperature is very large compared to the flow velocity (or more generally the random component dominates over the correlated one) the average emission point is zero (center of the source). If this happens for both particles, the asymmetry is zero. If it happens for only one of them, the asymmetry exists. If the flow velocity strongly dominates over temperature, and particles are emitted from the same system, both average emission points are strongly shifted by the same amount and in consequence the asymmetry is again small. From the discussion we see that the existence of emission asymmetry is not trivial and only arises in a sys-

² We have chosen the convention to always take the lighter particle as first in the pair.

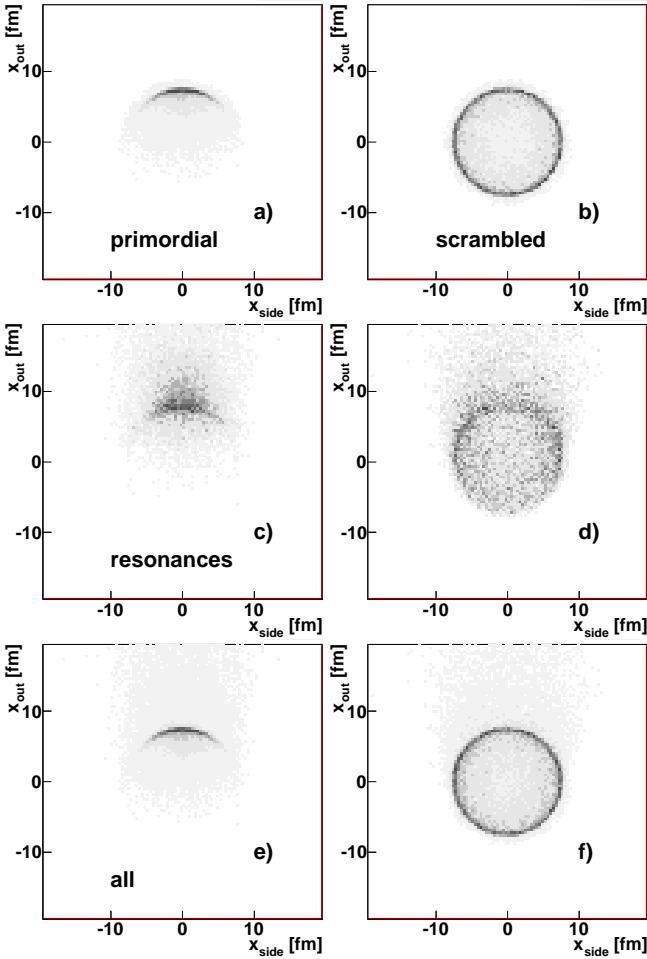


FIG. 4: Emission points of particles with the velocity in (0.6, 0.8), its direction pointing “upwards”, for protons, central Au+Au. Panels notation the same as in Fig. 2.

tem where both random(thermal) and correlated(flow) velocities exist and are comparable in magnitude.

We will illustrate the consequences that this mechanism has for the particle’s emitting regions using the THERMINATOR calculations for central Au+Au collisions at the top RHIC energy as an example. First, we focus on the “primordial” particles, that is particles coming directly from the hydrodynamical stage. Let us consider two variables:

$$\begin{aligned} x_{out} &= \mathbf{x} \mathbf{p}_T / p_T \\ x_{side} &= \mathbf{x} \times \mathbf{p}_T / p_T. \end{aligned} \quad (6)$$

The first one is the component of the particle’s transverse emission vector parallel to the particle’s transverse momentum; the other is the perpendicular component. In the upper-left panel of Fig. 2 the distribution of these emission components are shown for primordial kaons. A strong correlation is seen - all particles moving “upwards” (to the positive “out” direction) are emitted from the positive x_{out} part of the source. This focusing of particle’s emission has two distinct effects: the overall size

of the emitting region shrinks both in the “out” and the “side” direction and the average emission position shifts in the “out” direction, but not in “side”. Looking at the upper-left panel of Fig. 3 one sees the same effects but to a much smaller degree for pions with the same *velocity*: the size is shrunk, but not as much, the average emission position is also shifted but by a smaller amount. The exact numerical values for the “size” (or variance) and “shift” (or mean) of these distributions can be found in Tab. II. Fig. 4 shows analogous pictures for protons. As expected, the effect is the strongest here, as protons have almost twice the mass of kaons.

From the discussion above, and the numerical values in Tab. II and III, one immediately sees that hydrodynamics produces two distinct trends in femtoscopic observables: (a) The size of the emitting system gets smaller with increasing p_T of the particle. This effect is well understood theoretically (so called “lengths of homogeneity”) and universally observed experimentally in femtoscopy in heavy-ion collisions (“ m_T scaling”) [24]. (b) Average emission points of particles with different p_T (for example with same velocity but different mass) are different, and this difference is well defined: lighter particles appear to be, on average, emitted closer to the center of the source³.

The second trend is the main focus of non-identical particle analysis. It so happens, that the non-identical particle femtoscopy correlates particles with *the same velocity* but possibly with *different masses*. Moreover, it has a unique feature of being able to measure not only the “size” (more precisely - the second moment of the two-particle distribution - the variance) but also the “shift” (i.e. the first moment of the distribution - the mean) between average emission points. It is therefore able to directly test the predictions of the hydrodynamic model with respect to the $x - p$ correlations. We would like to emphasize that this is the most direct and unambiguous signal of collectivity available to femtoscopy. The m_T scaling, which is predicted by hydrodynamics, can also be explained by other mechanisms not requiring collectivity (e.g. “temperature gradients” [34]); but no mechanism is known, which would produce such specific emission asymmetries with no collectivity.

The asymmetry is predicted to arise only in the “out” direction. The “side” asymmetry is zero. It can also be shown that for rapidity symmetric systems of a collider, such as RHIC, when the target is identical to the projectile, the longitudinal asymmetry is also expected to vanish.

³ Note that the values in Tab II are calculated vs. the single-particle momentum direction, which is only the approximation of the *out* direction. Values in Tab. III are calculated vs. the proper *out* direction - the total momentum of the pair. Therefore small differences between the shift values in the two tables are to be expected.

B. “No directional correlation” test

In the last section we have argued that the correlation between spatial emission angle ϕ_r and particle’s velocity direction ϕ_f is responsible for the emission asymmetries. We have tested this argument by performing a calculation in which we have intentionally broken this correlation, in order to show that in such case no asymmetries arise. We take each *primordial* particle separately. From its original transverse emission coordinates (x_o, y_o) we calculate its transverse emission radius r and angle ϕ_r . Then, we randomize the angle ϕ_r , but keep the emission radius r unchanged, and calculate the new “scrambled” emission point (x_s, y_s) . If the particle is unstable and consequently decays, the emission points of all daughter particles are shifted by the same amount, calculated for the parent particle $(x_s - x_o, y_s - y_o)$. Note that the momentum observables are not affected.

The upper-right panels of Figs. 2, 3 and 4 show the effect of this procedure on primordial particles. As expected, the average emission point of all particle types is now at $(0, 0)$, and the asymmetry between particles of different masses, shown in Tab. III is zero. Our claims are confirmed: the model with no directional correlation shows no asymmetry.

C. Importance of resonances

The Lhyquid+THERMINATOR model assumes that the evolution of the heavy-ion collision proceeds in stages. After the initial non-equilibrium phase there is a collective phase, which can be well described by hydrodynamic equations, with the equation of state assuming the existence of the Quark Gluon Plasma. However, at some point the system becomes so dilute that the continuous medium description of hydrodynamics is no longer viable and one converts the system to hadronic degrees of freedom - the THERMINATOR model does it via the von-Neumann sampling of the probability distribution obtained from the Cooper-Frye formula. All known resonances are the degrees of freedom in the hadronic phase. Their abundances are well described by chemical models, and if one trusts these calculations, then at least 2/3 of the observed pions do not come from the original hydrodynamic phase (the so-called “primordial” particles), but are daughters of resonances. Additionally all resonances have their intrinsic lifetime, so they travel some distance before decaying - hence they will certainly modify the space-time picture of particle emission. It is clear that a careful and detailed simulation of the resonance propagation and decay (e.g. as implemented in THERMINATOR) is a critical feature of the model which aims to describe femtosopic observables. Also, the relative abundances and decay momenta of resonances producing pions, kaons and protons as final particles are obviously quite different; so, the feature is even more important for non-identical particle correlations, where we study relative differences

between various particle types.

Let us first qualitatively consider a resonance decay process. We have the original resonance, produced as a primordial particle. Its emission followed common “flow” $x - p$ correlation, as for any other particle. Resonances are usually quite heavy, so we expect this correlation to be strong. The resonance travels some distance with the original velocity - this enhances the $x - p$ correlation. After some random time the decay process occurs. Two (or three) particles are created at the decay point. We note the similarity between the resonance decay process and the emission from the fluid element. The daughters of the resonance will have the “common” velocity - this time it is not the fluid elements velocity, but simply the resonance’s one. And they will have the “random” component - the “decay momentum” of the given decay channel. And again the random component will matter more for the lighter particle - the velocity that corresponds to the fixed “decay momentum” will be larger for the lighter particle. One can imagine two scenarios. If the decay momentum of the given decay channel is large, compared to the daughters’ mass, than the daughters’ emission direction will be randomized, and the common $x - p$ correlation will be lost. On the other hand if the decay momentum is small, the correlation will be preserved (or, in other words, the daughter particle will travel in roughly the same direction as the parent) or even enhanced due to the additional $x - p$ correlation resulting from resonance propagation.

From the description above one concludes that the resonance process will induce the space-momentum correlation in a way similar to the collective flow; so, one can ask if it can be an alternative mechanism producing such asymmetries. However, qualitative expectations for values of the asymmetries or even general trends are not immediately obvious. They will non-trivially depend on relative abundances of resonances and their daughters, as well as particular values of decay momenta in specific decay channels. The fact that some resonances decay in cascades makes it even more complicated [75]. Moreover the original primordial resonances will have a natural $x - p$ correlation coming from the earlier hydrodynamic phase. One then faces a quantitative problem: do the resonance decays introduce emission asymmetries on their own, independent from flow asymmetries? And if yes, how big are they, compared to the asymmetries coming from flow? In particular are they small enough, so that one can still safely interpret the asymmetry observed in the experiment as coming from collective behaviour such as flow?

To answer these questions a detailed simulation is needed, in particular one that has intrinsic $x - p$ correlations coming from flow (preferably with the possibility to switch them off) and which incorporates all known resonances, together with the state-of-the art knowledge of their masses and decay channels. From this description it is clear that THERMINATOR model is perfectly suited for the task. In addition, we use the “scrambling” procedure described in the previous Section to switch off the $x - p$

correlations coming from flow, in order to estimate the asymmetry coming from the decay processes alone.

Let us see what is the effect of resonance decays on the properties of the emitting regions. In panels e) of Figs. 3, 2, 4 the emission points of all particles (both primordial and from resonances) are shown, while Tab. II shows the numerical values of sizes and shifts. The resulting asymmetries are listed in Tab. III. We consider the size of the system first. As expected the overall size is larger - that is naturally expected as the resonances travel some distance before they decay. The m_T scaling seems to be preserved. In general the trend is consistent with previous studies of resonance influence on femtoscopic observables [53, 75] and agrees with the natural expectations. Less trivial and more interesting effects are visible in the average emission points. A qualitatively different effect is seen for pions than for kaons and protons. We first inspect the emission points for particles coming from resonances only (no primordial ones), seen in panels c) of Figs. 3, 2, 4. For pions the average emission point is shifted *less* from the center for resonance daughters, than for the primordial ones. Apparently the first scenario described three paragraphs before is in effect here: the decay momenta of the resonances producing pions are so large, compared to the pion mass, that they completely wash out the original flow $x - p$ correlation. In contrast both for kaons and protons the resonance daughters are shifted *more* from the center than primordial particles. This time the second scenario is in effect - the decay momenta are small compared to particles' masses, so small, in fact, that they are not even able to counter the additional $x - p$ correlation coming from resonance propagation. A more detailed discussion of this effect, with examples of particular resonances and decay channels for pions and kaons is found in [76]. The effect persists when one takes all particles, primordial and resonance daughters, together. Both effects collaborate in enhancing the pion-kaon and pion-proton asymmetries:

$$\begin{aligned}\langle r_{out}^{\pi K} \rangle &\approx \langle x_{out}^{\pi} \rangle - \langle x_{out}^K \rangle \\ \langle r_{out}^{\pi p} \rangle &\approx \langle x_{out}^{\pi} \rangle - \langle x_{out}^p \rangle\end{aligned}\quad (7)$$

while the kaon-proton asymmetry stays rather similar to the primordial only case (and small):

$$\langle r_{out}^{Kp} \rangle \approx \langle x_{out}^K \rangle - \langle x_{out}^p \rangle. \quad (8)$$

We compare the source distributions in panels on the left in Figs. 3, 2, 4 to the ones in panels on the right, where the “scrambling” procedure was applied. The numerical values for asymmetries are given in Tab. III. First, let us focus on pion-kaon and pion-proton pairs. As already discussed, “scrambled” primordial particles show no asymmetry. The non-primordial ones do show some, but still significantly lower than the non-scrambled ones. This shows that for non-primordial particles *both* sources of asymmetry are important: the original $x - p$ correlation of the parent particle and the additional asymmetry

TABLE IV: Time and space asymmetries (from the fits to the distributions around their peaks) for central Au+Au collisions. PRF values are with asterisk.

	$\langle r_{out} \rangle$	$\langle \gamma_t \rangle \langle r_{out} \rangle$	$\langle \Delta t \rangle$	$-\langle \beta_t \rangle \langle \gamma_t \rangle \langle \Delta t \rangle$	$\langle r_{out}^* \rangle$
πK all	-3.3	-5.0	2.7	-3.0	-8.0
πK pri	-1.6	-2.4	1.5	-1.7	-4.1
πp all	-4.0	-5.7	3.8	-3.5	-9.2
πp pri	-2.4	-3.4	2.1	-2.0	-5.4
Kp all	-0.8	-1.1	0.9	-0.6	-1.7
Kp pri	-1.0	-1.3	0.5	-0.4	-1.7

from the decay process. However, the former dominates. A critical test is the comparison of asymmetries for all particles between normal “flow” and “scrambled” scenarios, since this is the observable measured in the experiment. As the simulation shows, the asymmetry which can be attributed solely to the trivial resonance decay processes can account for only 20% (17%) of the total asymmetry produced in central Au+Au collisions at top RHIC energy for the pion-kaon (pion-proton) pair. For kaon-proton the additional asymmetry produced by the resonance decays is negligible.

In summary, we have shown that resonance decays do not dilute, but rather enhance the asymmetry signal for pion-kaon and pion-proton pairs. At the same time, even though the resonance decay process can potentially be an independent source of emission asymmetry, we have shown, by detailed calculations, that in realistic conditions such asymmetry is less than a quarter of that produced by flow. Therefore our original expectation holds: if significant emission asymmetry is observed in pion-kaon and pion-proton correlations in the experiment, it favors the explanation of strong $x - p$ correlations in the emitting system, such as the ones produced by hydrodynamic radial flow.

D. Flow versus time asymmetries

As we have noted in the Introduction, the non-identical particle correlations technique has been initially developed to measure mainly the emission time differences between various particle species. Only later the connection to radial flow was noted [9, 35].

In Au+Au collisions one expects intrinsic time differences for at least two reasons. The reader is referred to [50], where the evolution of the average emission times with particle's p_T was discussed. It was noted that due to the particular features of the hydrodynamic emission function, particles with larger p_T were, on average, emitted earlier. In addition, studies with the “blast-wave” parametrization [42] showed that a time difference between particles of different masses arises in boost-invariant models (the influence of the violation of boost invariance on the time and longitudinal shifts has been discussed in [74]). In our case both effects would con-

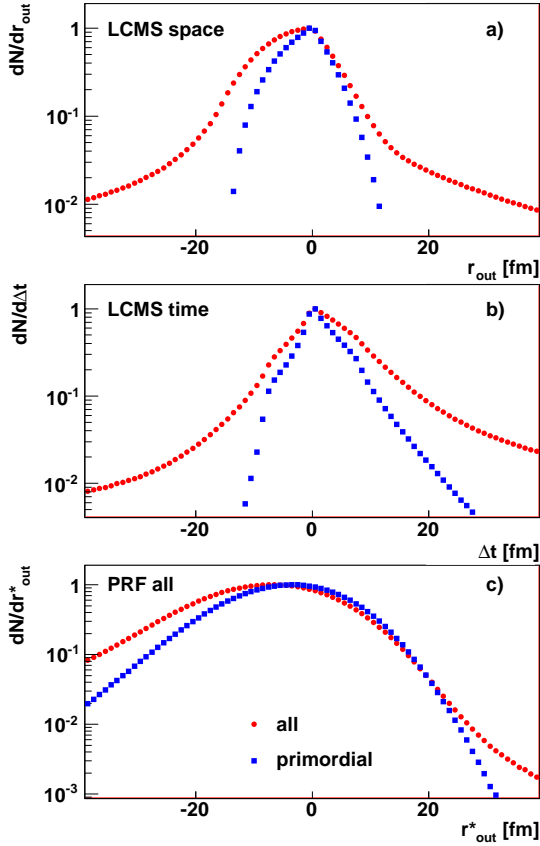


FIG. 5: (Color on-line) Pion-kaon emission functions in LCMS for space a) and time b) components, combined into the observable asymmetry in PRF c). Red circles are for all particles, blue squares for primordial only.

tribute to the additional asymmetry in PRF:

$$r_{out}^* = \gamma_t (r_{out} - \beta_t \Delta t), \quad (9)$$

which would go *in the same direction* as the spatial one coming from radial flow. Even though it cannot be directly correlated with the radial flow, it is still very much hydrodynamic in nature and we do not consider it as an alternative, non-collective explanation of the asymmetry.

However, the resonance decay process can also introduce additional time asymmetries, as resonance decays occur with a certain time delay and if some particles are more abundantly produced by resonances than others, asymmetries may arise. In contrast to the effect discussed in the previous paragraph, these time delays are not “hydrodynamic” in nature and should be treated as alternative sources of asymmetry. Moreover, one expects pions to be most abundantly produced by resonance decays, which would mean that they would appear to be, on average, produced later than kaons and protons, producing asymmetry *in the same direction* as the flow. Clearly the matter requires careful quantitative study.

In Fig. 5 the time and space emission asymmetries are shown on the left and central panels. One sees that both are present and are significant. Resonance decays modify both distributions and add a complication of long-range

tails. Therefore, a simple mean of a distribution is no longer a good variable to characterize such asymmetries. One is forced to use the mean values of the functional forms fitted to the distributions around the peak. Tab. IV shows the summary of these fits. We see that even for the primordial particles only, there is already a time difference, although smaller than the space one. Introducing resonances increases the time asymmetry. Evidently the expected effect is seen. Comparing the values in PRF we take the difference between “all” and “primordial” cases for the time asymmetry as an estimate on how much time asymmetry the resonance decays introduce. Both for pion-kaon and pion-proton the “non-hydrodynamic” asymmetry coming purely from resonance time delay is less than 15% of the predicted overall asymmetry. For kaon-proton it is less than 25%. Again, the flow asymmetry dominates the calculated asymmetry signal.

E. Expectations for qualitative trends

Following the discussion in the previous subsections one can formulate several predictions of expected qualitative trends. We will consider pions, kaons and protons in specific p_T windows, corresponding to the acceptance of the STAR experiment at RHIC. This means that the velocities of these particles will be fixed, and one might assume that the same pions will be correlated with kaons for the pion-kaon correlation and with the protons for the pion-proton correlation. Since we are correlating particles with similar velocity, we will be correlating very low- p_T (≈ 0.1 GeV/c) pions with medium- p_T kaons (≈ 0.5 GeV/c) and moderate- p_T protons (≈ 1 GeV/c). We give a detailed relation between single-particle and two-particle sizes in Appendix A. In terms of the observables themselves, that is the two particle variances, one expects that $R_{\pi K}$ and $R_{\pi p}$ will be similar and large, since they are dominated by the large low- p_T pion size. In contrast R_{Kp} is expected to be significantly smaller.

The asymmetries show a common feature - with the definition of Eqs. (7),(8) (the lighter particle always taken as first) they are all negative - which reflects the fact that lighter particles are expected to be emitted closer to the center of the system than the heavier ones.

As for the relations between asymmetries, hydrodynamics naturally predicts that the $\mu_{\pi p}$ will be the largest, $\mu_{\pi K}$ will be of similar magnitude but smaller, while μ_{Kp} will be much smaller than the other two. It can also be shown that the following relation should hold:

$$\mu_{\pi p} = \mu_{\pi K} + \mu_{Kp} \quad (10)$$

The asymmetries for “all” particles for pion-kaon and pion-proton pairs should be significantly different than for “primordial” only, while for kaon-proton the difference should be small.

In Figs. 6, 7, 8 the predicted system size and emission asymmetry for pion-kaon, pion-proton and kaon-proton

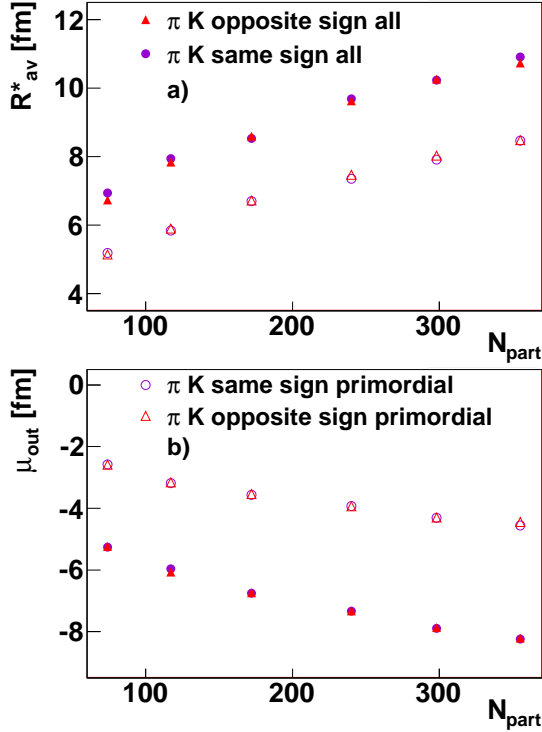


FIG. 6: (Color on-line) The pion-kaon overall radius a) and emission asymmetry b) in PRF as a function of centrality for Au+Au collisions at $\sqrt{s_{NN}} = 200$ GeV. Close points are for all particles, open for primordial only. Circles are same-sign pairs, triangles - opposite-sign.

pairs respectively, calculated by Lhyquid+THERMINATOR, are shown. All the expected trends mentioned in this section are confirmed.

F. Centrality dependence

We first consider the centrality dependence of the system size. The assumed initial conditions have a clear dependence: the system size and initial temperature grow with N_{part} ; both should result in larger sizes thorough of the evolution. The hydrodynamic evolution assumes identical equation of state and identical freeze-out temperature for all centralities; so, there is no reason to expect that this dependence will be altered in the final state. Also, calculations for identical pions show the same trend. Finally, all available experimental data, including pion, kaon and proton femtoscopy show the same trend. Therefore increase of the system size with N_{part} is expected.

The asymmetry is the result of a hydrodynamic evolution. As already mentioned the parameters of the evolution do not change with centrality, only the initial conditions. Since the chemical properties of matter do not depend on centrality either, the resonance decay phase is not expected to be very different, giving an enlargement of the system size by a constant amount. On the

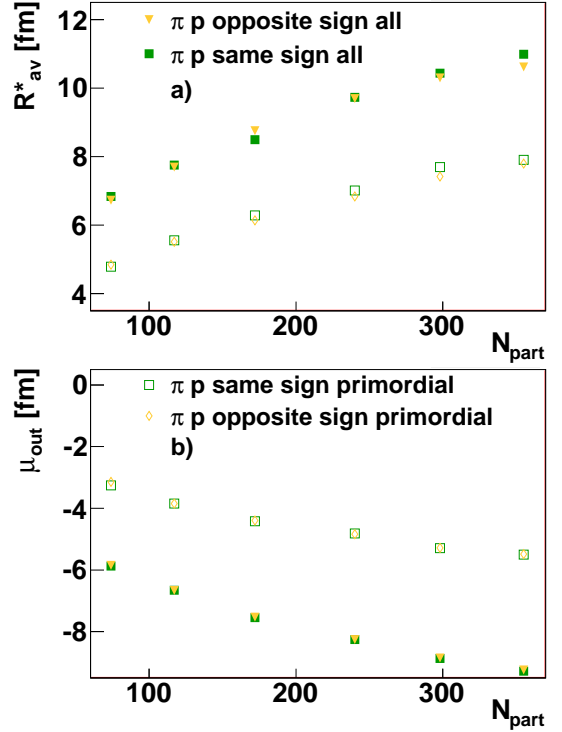


FIG. 7: (Color on-line) The pion-proton overall radius a) and emission asymmetry b) in PRF as a function of centrality. Close points are for all particles, open for primordial only. Squares are same-sign pairs, triangles (diamonds) - opposite-sign.

other hand, as the collisions become more peripheral, the initial overlap region is shrinking, so one expects that the long-range resonance corona will become relatively more important. Since we know that the overall size of the system grows with centrality, the absolute value of asymmetry will also grow. The ratio of asymmetry to the system size is shown in Fig. 9 and indeed we can see that the scaling of μ with R_{av}^* holds well for all centralities, all pair types, both for “all” and “primordial only” particles.

IV. NON-IDENTICAL PARTICLE FEMTOSCOPY FORMALISM

In femtoscopy one aims to measure the space-time configuration of the emission process in hadronic collisions by analyzing the specific behavior of the two-particle correlation function. A natural variable versus which this correlation is measured is the half of generalized pair relative momentum k^* , as opposed to analyses focused on event structures, which use e.g. azimuthal angle and pseudorapidity differences. k^* is calculated in the pair rest frame, so it is also the momentum of the “first” particle of the pair in the PRF. The particles in the pair are different, so it is important to define which one is “first”. Later we give the conventions which we use in this paper.

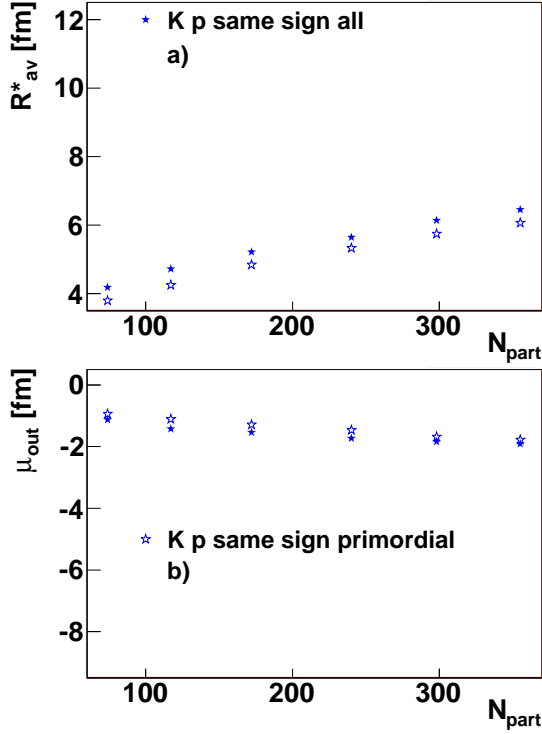


FIG. 8: (Color on-line) The kaon-proton overall radius a) and emission asymmetry b) in PRF as a function of centrality. Close points are for all particles, open for primordial only.

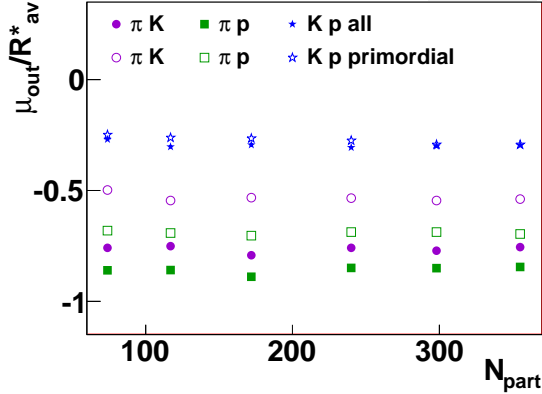


FIG. 9: (Color on-line) The emission asymmetry scaled by the overall system size in PRF. Closed points are for all particles, open for primordial only. Circles are for pion-kaon pairs, squares for pion-proton, stars for kaon-proton.

Femtoscopy also requires a precise knowledge of particle type, which means experiments wishing to do such analysis must have good particle identification capability.

The correlation function is defined as:

$$C(\mathbf{p}_a, \mathbf{p}_b) = \frac{P_2(\mathbf{p}_a, \mathbf{p}_b)}{P_1(\mathbf{p}_a)P_1(\mathbf{p}_b)}, \quad (11)$$

where P_2 is a conditional probability to observe a particle with momentum \mathbf{p}_b if a particle of momentum \mathbf{p}_a was also observed, while P_1 is a simple probability to observe a particle with a given momentum. Note that this

definition is general and applies equally well to the femtosopic correlation function and to other two particle correlations e.g. event structure ones.

The experimental femtosopic correlation function is a specific form of Eq. (11), written as:

$$C(\mathbf{k}^*) = \frac{\int A(\mathbf{p}_a, \mathbf{p}_b) \delta(\mathbf{k}^* - \frac{1}{2}(\mathbf{p}_a^* - \mathbf{p}_b^*)) d^3 p_a d^3 p_b}{\int B(\mathbf{p}_a, \mathbf{p}_b) \delta(\mathbf{k}^* - \frac{1}{2}(\mathbf{p}_a^* - \mathbf{p}_b^*)) d^3 p_a d^3 p_b} \equiv \frac{A(\mathbf{k}^*)}{B(\mathbf{k}^*)}, \quad (12)$$

where $A(\mathbf{p}_a, \mathbf{p}_b)$ is the distribution of correlated pairs (i.e. both particles coming from the same event) of particles of type a and b and $B(\mathbf{p}_a, \mathbf{p}_b)$ is the same distribution, but particles are not correlated (i.e. come from two different events). Note that the argument of C is changed to half of the pair relative momentum \mathbf{k}^* . Also note that with this definition the correlation function will contain not only femtosopic correlations, but also all other event-wide correlations projected to the two-particle space. These include: elliptic flow v_2 , global event energy and momentum conservation, resonance decay correlations (if a and b are different and can be products of the decay of a given resonance, e.g. products of the Δ^{++} resonance in the $\pi^+ - p$ correlation function), residual correlations (remnants of the femtosopic correlations between parent particles, which decayed weakly into the particles of interest, e.g. residual correlations between Λ and p feeding into the $p-p$ correlations), jets, etc. There are numerous experimentalists recipes to construct B in such a way that these correlations are included there. In that case, dividing A and B also divides out the correlations. One should also correct for other non-femtosopic effects, so that one is left with pure femtosopic correlation in C . The latter is desirable, since it is the femtosopic-only effect that is usually computed in models. But such correction procedures are never fully effective; so, one must take it into account when comparing the “compound” correlation functions from the experiment with the “pure” femtosopic CF from models. The details of such procedures are clearly experiment dependent and are beyond the scope of this paper. We only note that some models may include the effects of global correlations (e.g. elliptic flow, energy-momentum conservation); so, they can be used to model such effects. We discuss how this can be done later in the chapter.

In models one defines the correlation function via the single and two-particle emission functions:

$$S_A(\mathbf{x}_1, \mathbf{p}_1) = \int S(x_1, p_1, x_2, p_2, \dots, x_N, p_N) dx_2 dp_2 \dots dx_N dp_N \quad (13)$$

$$S_{AB}(\mathbf{x}_1, \mathbf{p}_1, \mathbf{x}_2, \mathbf{p}_2) = \int S(x_1, p_1, x_2, p_2, \dots, x_N, p_N) dx_3 dp_3 \dots dx_N dp_N \quad (14)$$

which are interpreted as a probability to emit a particle (a pair of particles) from a given space-time point with

a given momentum. With this definition one might substitute S_{AB} for P_2 and S_A for P_1 in (11). Such a correlation function is a 14-dimensional object (7 independent components per particle: 4 space-time and 3 momenta). Assumptions are needed to reduce the number of dimensions. We describe them below.

In principle, the source emission function S_{AB} should reflect all the physics aspects of the particle emission process, including the proper symmetrization for bosons and fermions, as well as the influence of the two-body and many-body Final State Interaction (FSI). However, commonly used heavy-ion collision models do not include these effects. Instead, one assumes that each particle's emission process is independent, or in other words that an interaction between the two final-state particles after they are created is independent from their emission process. The introduction of this factorization of the FSI and two-particle wave function symmetrization gives the equation:

$$C(\mathbf{p}_1, \mathbf{p}_2) = \int S_{AB}(\mathbf{p}_1, \mathbf{x}_1, \mathbf{p}_2, \mathbf{x}_2) |\Psi_{AB}|^2 d^4\mathbf{x}_1 d^4\mathbf{x}_2 \quad (15)$$

where Ψ is the pair wave function. Particle types A and B are known, so the momenta have only three independent components, while for positions all four components are independent. We also mention that the equation (15) has strong similarities to the Fermi equation used to describe the β decay process [77].

A. Pair wave function

The pair wave function Ψ describes the behavior of a pair of particles, one of type A and another of B . In non-identical particle correlations we use a particular form of Ψ , which corresponds to the following physical scenario: two particles A and B , which, shortly after they are produced in heavy-ion collision, interact via the FSI, in our case Coulomb and/or Strong. After this interaction they propagate to the detector as plane-waves. In that case, the particular form of Ψ is the solution of the scattering problem, viewed with the reversed time direction. We also use equal time approximation which assumes the particles were born at the same time in PRF (see [10, 14] for a detailed description and estimation of the systematic error introduced by such assumption). We factorize the wave function into the part describing the motion of the pair as a whole (a function of pair total momentum and “average” emission point), and the component describing the interaction itself – dependent on pair relative momentum \mathbf{k}^* and separation \mathbf{r}^* . The first component produces only an additional phase, which does not influence the modulus of the wave function. Since in our study we are only interested in the modulus, we can

neglect this component, and we are left with [10]:

$$\Psi_{-k^*}^{(+)}(\mathbf{r}^*) = \sqrt{A_C(\eta)} \left[e^{-i\mathbf{k}^* \cdot \mathbf{r}^*} F(-i\eta, 1, i\zeta) + f_C(\mathbf{k}^*) \frac{\tilde{G}(\rho, \eta)}{\mathbf{r}^*} \right] \quad (16)$$

where A_C is the Gamow factor, $\zeta = k^* r^* (1 + \cos \theta^*)$, $\eta = 1/(k^* a_C)$, F is the confluent hypergeometric function, \tilde{G} is the combination of the regular and singular s-wave Coulomb functions and f_C is the strong scattering amplitude, modified by the Coulomb interaction. θ^* is the angle between the pair relative momentum \mathbf{k}^* and relative position \mathbf{r}^* in PRF, while a_C is the Bohr radius of the pair, equal to 248.52 fm, 222.56 fm and 83.59 fm for pion-kaon, pion-proton and kaon-proton pairs respectively, and is negative for opposite-charged pairs. For identical particles Ψ must also be properly (anti-)symmetrized. This equation is valid in the outer regions of the Strong Interaction potential, and neglects the components for angular momentum $l \geq 1$, the latter is a valid approximation for small k^* .

In femtoscopy analysis we assume that we know Ψ with infinite accuracy, so that we can try to invert Eq. (15) to obtain, from the measured correlation function C , the information about the emission function S_{AB} . In this work we focus on non-identical combinations of the most abundant stable hadrons measured in heavy-ion collisions: pions, kaons and protons. For each of the combinations (pion-kaon, pion-proton and kaon-proton) there are four charge combinations: two of the same sign and two of the opposite sign. The wave function for both same-sign (and both opposite-sign) combinations are identical. We note that the wave function characteristics are indeed well known for all combinations, except for the opposite-sign kaon-proton. The strong interaction in this system is interesting in its own right, and is the focus of intense theoretical investigation (see e.g. [78]). The femtoscopy technique can be useful in this regard – by inverting the problem and assuming that we know the source distribution (from other femtoscopy measurements) we can invert Eq. (15) to deduce the parameters of Ψ from the measured correlation function. Similar technique can also be used to study the strong interaction in the $\pi^+\pi^-$ system precisely. Such studies are beyond the scope of this paper (see, e.g., [10, 74]).

For the systems analyzed in this work, f_C can be parametrized in the effective range approximation by:

$$f_C(\mathbf{k}^*) = \left[\frac{1}{f_0} + \frac{1}{2} d_0 k^{*2} - \frac{2}{a_C} h(\mathbf{k}^* a_C) - i \mathbf{k}^* A_C(\mathbf{k}^*) \right]^{-1}, \quad (17)$$

where the f_0 is 0.137 fm for same-sign pion-kaon pair, -0.071 fm for opposite-sign pion-kaon pair, -0.148 fm for same-sign pion-proton, 0.112 fm for opposite-sign pion-proton, -0.360 fm for same-sign kaon-proton pair. The effective radius d_0 can be put equal to 0 for all considered pairs, at small k^* where the $1/f_0$ term dominates.

The full form of the wave function (16) must be used when calculating correlation functions to be compared

with data. However, for theoretical calculations it is sometimes instructive (and faster numerically) to neglect the strong interaction. This is acceptable since the strong interaction is expected to be small for the pairs of interest, except for opposite-sign kaon-proton pairs, which we will not include in the model calculations. For simplicity we will use the Coulomb-only wave function in the discussion in the next paragraph, but the conclusions hold for full Coulomb+strong wave function as well.

For the discussion it is important to provide the form of the F function explicitly:

$$F(\alpha, 1, z) = 1 + \alpha z + \alpha(\alpha + 1)z^2/2! + \dots \quad (18)$$

B. Emission function

The FSI correlation, described by (16), depends only on relative momentum \mathbf{k}^* and separation \mathbf{r}^* of the pair (the angle between the two vectors is θ^*). The first simplification of S_{AB} from (14) is to change to the relative variables and integrate out the sum ones:

$$\begin{aligned} S_{AB}(\mathbf{k}^*, \mathbf{r}^*) = & \int \int_{P_{min}}^{P_{max}} S_{AB}(\mathbf{x}_1, \mathbf{p}_1, \mathbf{x}_2, \mathbf{p}_2) \\ & \times \delta(\mathbf{k}^* - 1/2(\mathbf{p}_1^* - \mathbf{p}_2^*)) \\ & d^3 p_1 d^3 p_2 \\ & \times \delta(\mathbf{r}^* - (\mathbf{x}_1^* - \mathbf{x}_2^*)) \\ & d^4 x_1 d^4 x_2 \end{aligned} \quad (19)$$

The integration over space is done over the full variable range. On the other hand, particles' momenta are measurable, so it is possible to define the boundary momenta P_{min} and P_{max} for which the integration is done. In fact, for identical particle femtoscopy it is common to define several $k_T = 1/2(p_T^1 + p_T^2)$ ranges and create separate correlation functions for each of them. In this way, the information about the P dependence of S_{AB} is not completely integrated out and can still be inferred. Up to now similar binning was not possible for non-identical particle correlations at RHIC, because of small statistics and limited p_T acceptance with good PID coverage. However, when one compares the model and the experiment data, one must take care to restrict the P integration range at least to the one dictated by the p_T acceptance of the experiment.

The emission function (19) is a 7-dimensional object. We use it to rewrite the equation (15), putting the specific form of the wave function (16) as well:

$$C(\mathbf{k}^*) = \int S_{AB}(\mathbf{k}^*, \mathbf{r}^*) \left| \Psi_{-\mathbf{k}^*}^{(+),AB}(\mathbf{r}^*) \right|^2 d^4 \mathbf{r}^*. \quad (20)$$

This form can be explicitly used to calculate the correlation function from models. However, it is very rare for a model to provide the full two-particle emission function. The existing models fall into two categories: they

either provide an analytic form of a *single particle* emission function, or they provide information only about the produced particles.

In the first case we assume that each particle's emission process is independent. Then, the two-particle emission function S_{AB} can be constructed from single particle emission functions via a convolution:

$$\begin{aligned} S_{AB}(\mathbf{k}^*, \mathbf{r}^*) = & \int S_A(\mathbf{p}_1, \mathbf{x}_1) S_B(\mathbf{p}_2, \mathbf{x}_2) \\ & \times \delta(\mathbf{k}^* - \frac{1}{2}(\mathbf{p}_1 + \mathbf{p}_2)) \delta(\mathbf{r}^* - \mathbf{x}_1 + \mathbf{x}_2) \\ & \times d^4 \mathbf{x}_1 d^4 \mathbf{x}_2 d^3 \mathbf{p}_1 d^3 \mathbf{p}_2. \end{aligned} \quad (21)$$

In case of identical particles ($A \equiv B$) several simplifications can be made. The convolution of two identical Gaussians is also a Gaussian with σ multiplied by $\sqrt{2}$. Femtoscopy can provide information about the two-particle emission function only, but with the simplifying assumption above, the σ of the single particle distribution can be inferred. For non-identical particles, $A \neq B$, the above simplified method of comparison is not applicable. The comparisons with models is more complicated, but retrieving single-particle source sizes is still possible, provided a complete set of measurements is performed. The formula is used in Sec. VII and derived in Appendix A. Also, since generally $S_A \neq S_B$, the S_{AB} can yield a non-zero mean value of the separation vector $\langle \mathbf{r}^* \rangle$. Later in this Section we explain how this mean value can be accessed experimentally and argue that this is an important and unique piece of information accessible via non-identical particle femtoscopy only.

In the second case, of a model discretely producing particles, Eq. (20) is evaluated via the Monte-Carlo procedure:

$$C(\mathbf{k}^*) = \frac{\sum_{pairs} \delta(\mathbf{k}_{pair}^* - \mathbf{k}^*) \left| \Psi_{-\mathbf{k}^*}^{(+),AB}(\mathbf{r}^*) \right|^2}{\sum_{pairs} \delta(\mathbf{k}_{pair}^* - \mathbf{k}^*)}. \quad (22)$$

Note that if the particles from the model are produced in a correlated way (e.g. with energy and momentum conservation for the full event, with energy and momentum conservation for resonance decay, etc.) these are *not* destroyed and are still present in C . In other words, this method does not require the simplifying assumption of Eq. (21). In this work we use this method to calculate model correlation functions. Its practical implementation is described in Sec. V.

C. Correlation function and asymmetry signal

Eq. (15) essentially defines the correlation function as a pair wave function averaged over the source. Using the simplified wave function containing only the Coulomb part one can write:

$$C(k^*) = A_C(\eta)[1 + 2 \langle r^*(1 + \cos \theta^*) \rangle / a_c + \dots], \quad (23)$$

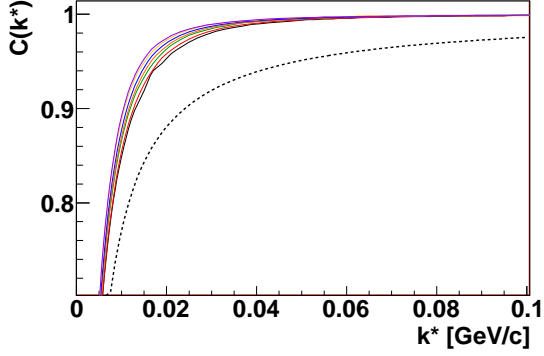


FIG. 10: (Color on-line) An example of the non-identical particle correlation function dependence on the size of the system. Solid lines represent same-sign pion-kaon correlation functions for a Gaussian source with sigma from 7.0 fm (lowest) to 13 fm (highest) and a shift of -5 fm. The Gamow factor is shown as a dashed line for comparison.

where averaging is done over pairs. In this example we illustrate the origins of the asymmetry effect by considering same-sign pion-kaon pairs. In such case, a_c is positive, A_C is negative and $r^*(1 + \cos\theta^*)$ is by definition always positive. For a point source ($r^* = 0$) the overall correlation effect $R = |C - 1|$ would be maximum and equal to $1 - A_C$. For our pairs $A_C - 1$ is negative, while $2 \langle r^*(1 + \cos\theta^*) \rangle / a_c$ is positive, so the two compete with each other. As the size of the system grows, so does average r^* , and the correlation effect R decreases. Therefore, the correlation function is sensitive to the source size; so, we expect to be able to measure the size of the system. One has to remember that as the size grows, the CF gets less and less sensitive to the system size; therefore, the analysis is able to accurately measure only sizes that are not too large. To determine whether the “too large” is larger than the maximum expected system size at RHIC is one of the objectives of this paper. Figure 10 shows an example of how a non-identical particle correlation function (in this case same-sign pion-kaon) depends on the size of the system. One can see that for a reasonable system size (comparable to the maximum femtoscopic sizes obtained in the central Au+Au collisions at RHIC) there is a noticeable and monotonic dependence on the size, indicating that a qualitative femtoscopic analysis should be possible.

As mentioned in the previous paragraph, the two-particle emission function can yield a non-zero mean value of the separation vector (\mathbf{r}^*). We now discuss how it can be observed in data. From Eq. (23) the correlation function depends on the angle θ^* , between relative momentum \mathbf{k}^* and relative position \mathbf{r}^* . When the two are aligned ($\cos\theta^* > 0$), the correlation effect is smaller, than when they are anti-aligned ($\cos\theta^* < 0$). The former configuration means that the particles of the pair, when born, immediately start to fly away from each other, so their effective interaction time is shorter. In the latter case, when they start to fly towards each other, pass

close to each other and only later fly away. Angle θ^* is not accessible experimentally, but it does influence R .

Particles’ momenta, measured experimentally, can be used to calculate the relative momentum \mathbf{k}^* and pair total momentum \mathbf{K} , corresponding to the velocity \mathbf{v} . The angle between the two is ψ . One divides the observed pairs in two groups: one having \mathbf{k}^* and \mathbf{v} aligned ($\cos\psi > 0$) and another, having \mathbf{k}^* and \mathbf{v} anti-aligned ($\cos\psi < 0$), and creates two correlation functions, C_+ and C_- . If in the pair sample used to calculate the C_+ we have a majority of pairs which also have $\cos\theta^* > 0$ (and in the C_- sample the majority of pairs have $\cos\theta^* < 0$), then C_+ and C_- would differ. In this particular case C_+ would show a smaller correlation effect and C_- a larger one. When plotting a “double-ratio” C_+/C_- one would see a signal deviating from unity. For same-sign pairs it would go above unity, while for opposite-sign pairs it would go below unity.

If we see a non-zero “double-ratio”, it means that $\cos\theta^*$ is somehow correlated with $\cos\psi$. They are connected via a third angle of interest: the angle ϕ between the pair velocity \mathbf{v} and the pair relative position \mathbf{r}^* . When we consider only the projections of all these angles on the transverse plane, we have trivially:

$$\psi = \theta^* + \phi. \quad (24)$$

For the average cosines of these angles, we can write:

$$\langle \cos\psi \rangle = \langle \cos\theta^* \cos\phi \rangle. \quad (25)$$

By definition for C_+ the left-hand side of Eq.(25) is positive. We assumed that C_+ shows larger correlation effect, so $\langle \cos\theta^* \rangle$ is negative. The only way that the equation can be fulfilled is to also have $\cos\phi < 0$. In other words it is required that, on average, \mathbf{r}^* is anti-aligned with \mathbf{v} . This is a crucial point, so let us restate it. If we see a non-unity double ratio we can conclude that the average relative position direction is correlated with the pair velocity direction. That means that we can access, via a rather straightforward procedure, the mean of the two-particle separation distribution, which is allowed to be non-zero for non-identical particles. The emission asymmetry $\langle \mathbf{r}^* \rangle$ is a three-vector, while the consideration above only mentions a single direction (the direction of the pair velocity \mathbf{v}). The argument is more general: we can replace \mathbf{v} by any other direction, defined in the Pair Rest Frame, and repeat the argument to obtain the same conclusions. The simplest generalization, which we have shown to have important physics motivation, is the decomposition of \mathbf{v} into components: the longitudinal “long” (along the beam axis) and transverse “out” (perpendicular to the beam axis). By performing the asymmetry analysis versus these two directions we can obtain information about the “out” asymmetry $\mu_{out} = \langle r_{out}^* \rangle$ and the “long” asymmetry $\mu_{long} = \langle r_{long}^* \rangle$. For completeness we also use the third direction: “sideways” or “side”, perpendicular to the other two to study the “side”

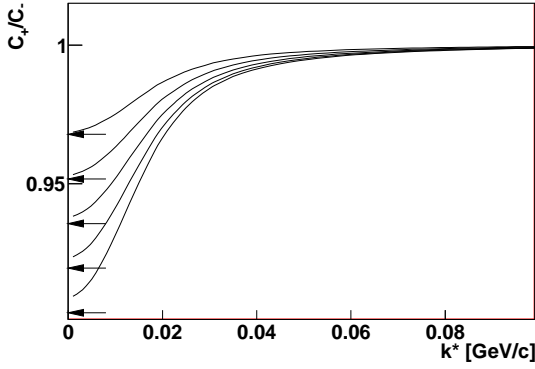


FIG. 11: An example of the non-identical particle “double-ratio” dependence on the emission asymmetry. Solid lines represent same-sign pion-kaon “double-ratios” for a Gaussian source with sigma of 10.0 fm and the asymmetry of -12.0 fm (lowest) to -4 fm (highest). The arrows show the asymptotic values (see text for details).

asymmetry $\mu_{side} = \langle r_{side}^* \rangle$. Each of them carries important physics information or is useful as an experimental cross-check; the details will be discussed in the following Sections.

We discussed the possible physical origins of the emission point asymmetry and its significance in Section III. Now we discuss the general properties of the “double-ratio” observable. It is allowed to go both above and below unity, which means either positive or negative emission asymmetry (the average emission separation being aligned or anti-aligned with the velocity direction). It can also be unity, meaning no emission asymmetry. More detailed analysis also shows that, for a fixed source size, introducing larger and larger emission asymmetry produces larger and larger deviation from unity of the “double-ratio” signal. This means that one can determine the existence of emission asymmetry and also measure its magnitude. The technical details of how it is done are presented in the next Section. The illustration of the “double-ratio” behavior, for a fixed system size for same-sign pion-kaon pair, is shown in Fig. 11.

It is instructive to derive the equation for asymptotic behavior of the double ratio C_+/C_- at k^* going to zero [8, 9]. We focus on the function F . In this limit, we neglect all components with $1/a_C$ or $1/k^*$ in powers greater than 1. We have:

$$F = 1 + 2\frac{r^*}{a_C} + 2\frac{\mathbf{k}^* \cdot \mathbf{r}^*}{k^* a_C} + O\left[\left(\frac{1}{a_C}\right)^2\right] + O\left[\left(\frac{1}{k^*}\right)^2\right] + \dots \quad (26)$$

which gives the correlation function:

$$C|_{k^*} = \langle A_C F^* F \rangle \doteq A_C \left(1 + 2\frac{\langle r^* \rangle}{a_C} + 2\frac{\langle \mathbf{k}^* \cdot \mathbf{r}^* \rangle}{k^* a_C} \right). \quad (27)$$

One notes that:

$$\langle \mathbf{k}^* \cdot \mathbf{r}^* \rangle = \langle k_{out}^* r_{out}^* + k_L^* r_L^* \cos(\theta^* - \psi) \rangle = k^* \cos \psi \langle r_{out}^* \rangle. \quad (28)$$

We now consider C at a fixed k^* and $\cos(\psi)$:

$$C(k^*, \cos \psi) = A_C \left(1 + 2\frac{\langle r^* \rangle}{a_C} + 2\cos \psi \frac{\langle r_{out}^* \rangle}{a_C} \right), \quad (29)$$

and using the uniformity of $\cos \psi$ distribution for uncorrelated particles at small k^* we have:

$$\begin{aligned} C_+ &\doteq A_C \int_0^1 C(\cos \psi) d\cos \psi = 1 + 2\frac{\langle r^* \rangle}{a_C} + \frac{\langle r_{out}^* \rangle}{a_C} \\ C_- &\doteq A_C \int_{-1}^0 C(\cos \psi) d\cos \psi = 1 + 2\frac{\langle r^* \rangle}{a_C} - \frac{\langle r_{out}^* \rangle}{a_C} \\ \frac{C_+}{C_-}|_{k \rightarrow 0} &\doteq 1 + 2\frac{\langle r_{out}^* \rangle}{a_C}. \end{aligned} \quad (30)$$

These asymptotic values of the double-ratio are shown in Fig. 11 as arrows. The formula appears to give an easy way to extract an emission asymmetry without the need for tedious analysis. However, one must remember that in the experiment, the lower the k^* , the higher is the experimental uncertainty on the data point. This is because of statistics, which falls as k^{*2} , and because experimental effects like momentum resolution result in the largest systematic uncertainty in these bins. Therefore, one has to perform the full analysis of the double ratio in a broad range of k^* to reliably extract the asymmetry.

From Eqs. (30) one concludes that if one restricts the integrals in the definitions of $C_+(C_-)$ to a $\cos(\psi)$ range close to 1(−1) one will obtain an even larger asymmetry signal. However, in the experiment, the price to pay is the loss of statistics, and hence the significance of the signal. It can be shown that in order to maximize the significance of the signal one should perform the integrals over the full range of $\cos(\psi)$ (thus minimizing the statistical error) with the weight $\cos(\psi)$ [79, 80]. We come back to this crucial point in Section V A where we discuss the spherical harmonics representation of the correlation function, which happens to naturally introduce similar weighting [80, 81].

We finish this chapter by discussing the conventions used in the analysis. It is important to define and consistently use these conventions in all steps of the analysis. First, the order of particles in the pair is important for the definition of k^* and r^* because they are defined as the momentum and position of the *first* particle in the pair. We adopt a convention that the lighter particle in the pair is always taken as first. If both particles have equal mass, the positively charged one is taken as first. The second convention is the definition of the double ratio, which can either be C_+/C_- , or C_-/C_+ . We chose the former definition. We also note that in the spherical harmonics representation there is no need for such a convention. With these definitions the following general rules hold. Same-charge pairs have correlation functions going below unity, opposite-charge pairs above unity. That means that for a given source size asymmetry, the double ratio for same-sign pairs will be an inverse of the opposite-sign double-ratio. Finally, with these definitions, a “double ratio” below (above) unity means that

the lighter particle is emitted closer to the center of the system and/or later than the heavier one for same-sign (opposite-sign) pair.

V. PRACTICAL IMPLEMENTATION OF THE FORMALISM

When using a model that produces individual particles (such as THERMINATOR), the integration in Eq. (15) is performed via the Monte-Carlo method, iterating over particle pairs. In that case, the procedure to construct the correlation function closely resembles the experimental one. It enables the introduction of some experimental effects, such as acceptance or momentum resolution, in a straightforward way, as opposed to the purely analytical models where this is more difficult. Mathematically, the procedure is a combination of Eqs. (12) and (15):

$$C(\mathbf{k}^*) = \frac{\int A(\mathbf{k}^*, \mathbf{r}^*) |\Psi(\mathbf{k}^*, \mathbf{r}^*)|^2}{\int B(\mathbf{k}^*, \mathbf{r}^*)}. \quad (31)$$

Note that the A and B now depend on space-time coordinates \mathbf{r}^* as well, because we are using model data in which the emission points are known. Since we are dealing with pairs of individual particles we employ the Monte-Carlo procedure, which replaces the analytic integration by summing over pairs:

$$C(\mathbf{k}^*) = \frac{\sum_{Npairs} \delta(k_A^* - k^*) |\Psi(\mathbf{k}^*, \mathbf{r}^*)|^2}{\sum_{Dpairs} \delta(k_B^* - k^*)}, \quad (32)$$

where the two sums are performed over two sets of pairs N and D and the δ function ensures that only pairs with the correct relative momentum are taken. Note that there are two possible scenarios, both of which have slightly different interpretations and uses. One can perform the calculation using the same pairs for set N and D . Eq. (32) is then exactly equivalent to (15), but is done via Monte-Carlo integration. Another option is to take pairs from the same event as sample N and pairs of particles from different events as sample D . In that case, the correlation function C contains not only the femtoscopic effect but also all other event-wide correlations which are present in the model, projected to the two-particle space. It is therefore very useful for the experimentalists who can study the differences between the two to estimate the magnitude of the non-femtoscopic effects. The two cases have one more important difference. Usually the CF is constructed as a ratio of two histograms: N , a signal, which is filled with the weight $|\Psi|^2$ for every pair, and D , the background, which is filled with unity for each pair. The errorbars on $C = N/D$ have different meaning in the two cases. In the first one it is just the spread of the weight in a given sample. In the second case it is a true errorbar, comparable to the experimental one, since samples N and D are statistically independent. In this work we are using the first way to calculate the correlation

function, since we are not interested in non-femtoscopic correlations, but rather in physics effects accessible via femtoscropy.

A. Correlation function representation

Femtoscopic correlation functions have been represented in two main forms: as a 1-dimensional histogram with the magnitude of the relative momentum k^* or $q = 2k^*$ on the axis, or as a 3-dimensional histograms with k_{out}^* , k_{side}^* and k_{long}^* on the axes. For identical pion correlations it is also useful to use a 3D histogram with the relative momentum components q_{out} , q_{side} and q_{long} calculated in the LCMS. Note that out, side and long decomposition is possible also for pairs of non-identical particles; one has to use the generalized four-momentum variable \tilde{q} instead of q : $\tilde{q} = q - P(qP)/P^2$. The first form requires minimal statistics, but only allows to determine the 1D overall source size. The second one allows for the determination of sizes in all 3 directions, but requires significant statistics. Up to now, the non-identical correlation function was represented as a set of two 1-dimensional histograms - one for C_+ and one for C_- with respect to the “out” direction. This allowed for the determination of 1D source size and a study of the “double ratio” to access asymmetries. However, if one wanted to study “double ratios” for other directions (“side” and “long”), one needed to create separate sets of correlation functions.

Recently, a more advanced way of representing the correlation function, the Spherical Harmonics (SH), was proposed [82]. It has several important advantages. It encodes the full 3D information of the correlation in a set of 1D plots. Generally, this does not need to be an advantage, because a perfect representation of all the features of any 3D function requires an infinite set of l, m components (meaning: infinite set of 1D histograms). But it so happens that the intrinsic symmetries of a pair distribution in the femtoscopic analysis result in most of the l, m components to vanish. It has also been shown that out of these that do not vanish, only those with small l contain important information, which means that one can safely truncate the decomposition at a rather small l without the fear of losing any physics information. It is as if the spherical harmonics have been specifically designed to efficiently represent a femtoscopic correlation function.

The spherical harmonics representation has the advantages of both the 1D correlation function (because it requires less statistics) and a 3D one (because it encodes the important part of the 3D information). However, first attempts to apply the decomposition methods, which were developed for identical particles, to the non-identical particle correlations were not successful. Essentially, one had to first construct the numerator and denominator as 3D histograms (usually in $|\mathbf{q}|$, $\cos \theta_q$ and ϕ), then divide them and decompose the resulting 3D cor-

relation function, negating the low-statistics advantage of the 1D representation. The decomposition procedure also relied heavily on the symmetries present for identical correlations. This presented a problem for non-identical correlations, because their primary goal is to study the emission asymmetry. This breaks one of the symmetries present in identical analysis. Also, the single particle acceptance of some experiments produced “acceptance holes” i.e. regions of empty bins in the 3D function. Also, statistics for non-identical pairs were significantly lower than for pion-pion correlations, so filling all the bins in a 3D correlation function with significant number of pairs became a challenge. To solve these problems, a new technique to represent the correlation function in spherical harmonics was developed [83]. Both the numerator and denominator are stored directly in spherical harmonics (*not* as 3D histograms), and the procedure to calculate the CF directly from them (again, *not* involving any 3D histogram) has been presented [83]. An additional benefit of the method is that the covariances between all l, m components are explicitly taken into account. Unless otherwise noted, all further correlation functions presented in this work are represented using this method. We also recommend that experimental groups use this method.

As was the case for identical particle femtoscopy, the spherical harmonics representation turned out to have specific synergies with the non-identical femtoscopic correlation analysis. The important femtoscopic information is contained in only two l, m components, while the other two can be used as additional cross-checks of experimental procedures. If one wishes to analyze the full 3D information, one needs to analyze only two more l, m components – the rest can be essentially neglected as they should be consistent with zero, or they will not contain additional useful information.

We now investigate the important components of the SH decomposition and their sensitivity to femtoscopic information. We perform a simple calculation in which we assume the source to be a 3D Gaussian in the LCMS, having three different sizes R in three directions (*out*, *side* and *long*). It also has a non-zero mean value μ_{out} in the *out* direction:

$$S(\mathbf{r}) = \exp\left(-\frac{(r_{out} - \mu_{out})^2}{R_{out}^2} - \frac{r_{side}^2}{R_{side}^2} - \frac{r_{long}^2}{R_{long}^2}\right). \quad (33)$$

With this source function we perform the integration (15) to calculate the correlation function and present it in spherical harmonics representation. We expect that the main femtoscopic information is contained in the following components: C_0^0 , $\Re C_1^1$, $\Re C_0^2$ and $\Re C_2^2$.

To study the sensitivity to the source size we increase the overall size, but keep the radii ratios the same. The results are plotted in Fig. 12. All components show some sensitivity, but the C_0^0 is affected the most. In the next step (shown in Fig. 13) we keep the source size the same, while we increase the emission asymmetry (μ_{out}). The main sensitivity is in the $\Re C_1^1$ component. More importantly, no asymmetry results in vanishing $\Re C_1^1$, while

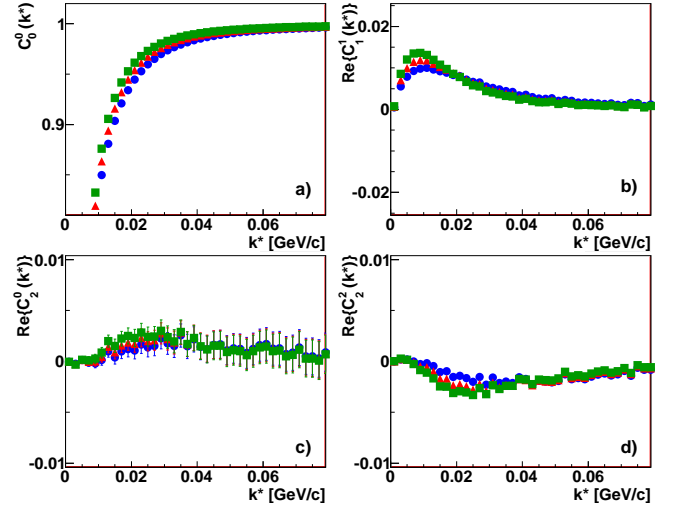


FIG. 12: (Color on-line) SH components of the correlation function for $R_{out} = 8$ fm, $R_{side} = R_{long} = 4$ fm, $\mu_{out} = -4$ fm (blue dots), $R_{out} = 10$ fm, $R_{side} = R_{long} = 5$ fm, $\mu_{out} = -5$ fm (red triangles), $R_{out} = 12$ fm, $R_{side} = R_{long} = 6$ fm, $\mu_{out} = -6$ fm (green squares).

increasing the asymmetry increases the signal in $\Re C_1^1$ monotonically, approximately linearly. $\Re C_1^1$ is functionally equivalent to the “out” double-ratio. Obtaining a quantitative as well as qualitative information about the asymmetry should be possible from the analysis of it (in correlation with at least C_0^0 where sensitivity is also seen, but to a smaller degree). In addition, from Eq. (30), we concluded that in order to maximize the significance of the asymmetry signal one should integrate the correlation function with the weight equal to $\cos(\psi)$ [79]. Remarkably, the definition of $\Re C_1^1$ is essentially:

$$\Re C_1^1(q) = N \int C(q, \cos(\theta_q), \phi_q) \sin(\theta_q) \cos(\phi_q) d\Omega_q, \quad (34)$$

where N is the normalization factor, while θ_q and ϕ_q are the longitudinal and transverse components of the ψ angle. The $\Re C_1^1$ component happens to be the optimal way to maximize the *transverse* components of the asymmetry signal, due to its $\cos(\phi_q)$ weight, while the $\Re C_1^0$ maximizes the longitudinal asymmetry signal, due to its $\cos(\theta_q)$ weight:

$$\Re C_1^0(q) = N \int C(q, \cos(\theta_q), \phi_q) \cos(\theta_q) d\Omega_q. \quad (35)$$

Once again it appears as if the spherical harmonics were specifically designed for the femtoscopic correlation function representation.

Next, in Fig. 14 we keep the transverse source size and the asymmetry the same, while we change the R_{long} radius. Obviously we see a change in the C_0^0 which reflects the growth of the overall system size. But the most sensitive component is $\Re C_2^2$ which carries information about the ratio of the transverse to the longitudinal radii, due to its $\cos^2(\theta_q)$ weighting.

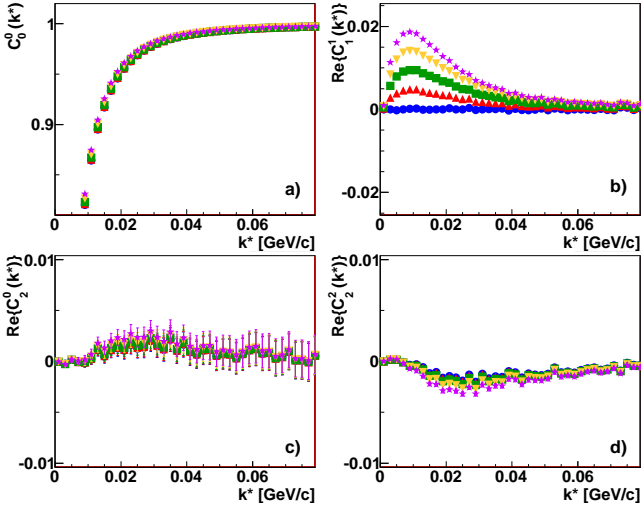


FIG. 13: (Color on-line) SH components of the correlation function for $R_{out} = 10$ fm, $R_{side} = R_{long} = 6$ fm. Emission asymmetry μ_{out} is changed from 0 fm (blue dots) via -2 fm (red up-triangles), -4 fm (green squares), -6 fm (yellow down-triangles), up to -8 fm (violet stars).

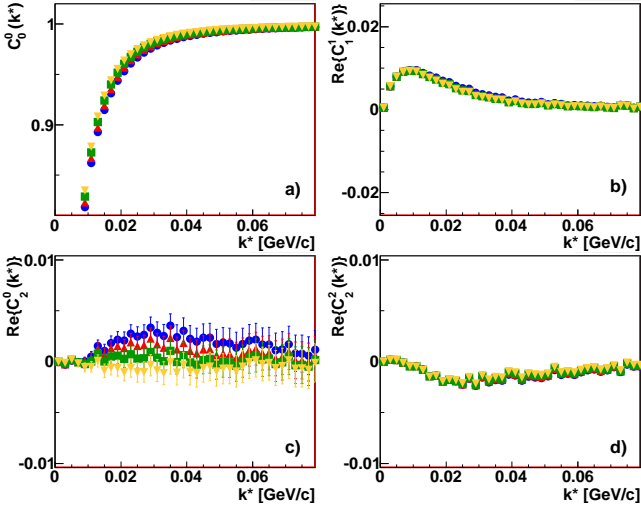


FIG. 14: (Color on-line) SH components of the correlation function for $R_{out} = 10$ fm, $R_{side} = 4$ fm, $\mu_{out} = -4$ fm. R_{long} is changed from 4 fm (blue dots) via 6 fm (red up-triangles), 8 fm (green squares) to 10 fm (yellow down-triangles).

Finally (see Fig. 15) we keep the sum of the transverse radii the same, but we change their ratio. The $\Re C_2^2$ component, with its $\cos^2(\phi_q)$ weighting, is the most sensitive to these changes, while the others remain practically constant.

The above calculations show that by analyzing just two components of the SH decomposition (C_0^0 and $\Re C_1^1$) one can already perform a meaningful femtoscopic analysis and determine the overall source size and emission asymmetry. Adding just two more components ($\Re C_2^0$ and $\Re C_2^2$), one can also determine source radii in all 3 directions, which would normally require a full analysis of a 3D correlation function. Full 3D analysis does require

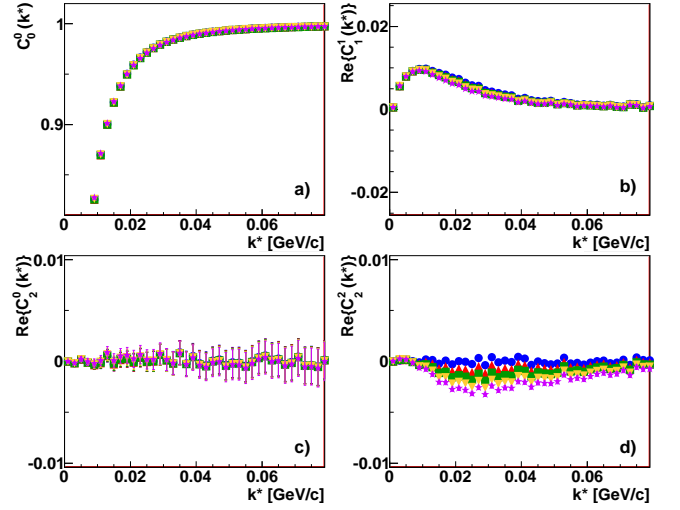


FIG. 15: (Color on-line) SH components of the correlation function for $R_{long} = 8$ fm, $\mu_{out} = -4$ fm. Transverse radii sum is kept constant: $R_{out} = 7$ fm, $R_{side} = 8$ fm (blue dots); $R_{out} = 8$ fm, $R_{side} = 7$ fm (red up-triangles); $R_{out} = 9$ fm, $R_{side} = 6$ fm (green squares); $R_{out} = 10$ fm, $R_{side} = 5$ fm (yellow down-triangles); $R_{out} = 11$ fm, $R_{side} = 4$ fm (violet stars).

larger statistics than the 1D size+asymmetry one, as the sensitivity to the observables in the $l = 2$ components is smaller than in the $l = 0$ and $l = 1$ ones. One should stress that in the SH representation one is dealing with 200 data points (50 points per histogram, 4 components) versus the 625000 bins in the 3D histogram representation. The huge savings in computation time and method complexity do not compromise the physics - one is able to obtain essentially the same femtoscopic information (3 sizes and emission asymmetry). It means that the 3D representation is a particularly inefficient way of storing the femtoscopic information, while the spherical harmonics one seems to be perfectly tailored for that task. We add that in all theoretical calculations that we have done all the other components were either required to vanish from symmetry relations, were consistent with zero, or contained femtoscopic information that was already accessible via the four main components. In experiment one should, in addition, look at the $\Re C_1^1$ (equivalent to the “long” double ratio) and $\Im C_1^1$ (equivalent to the “side” double-ratio). The former is expected to show zero asymmetry, the latter is required to vanish due to symmetry reasons, but their deviations from zero may signal experimental reconstruction problems.

B. Extracting qualitative information

In the previous paragraph the sensitivity of the non-identical particle correlation function to the source size and asymmetry was illustrated. Dependencies in Figs. 12, 13, 14, 15 show that source size parameters influence all SH components at the same time, and it is

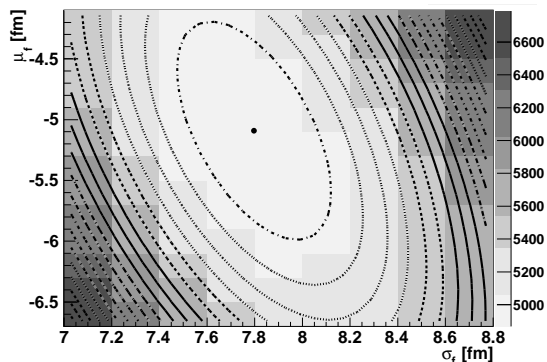


FIG. 16: (Color on-line) An example of the 2D χ^2 map obtained by fitting a non-identical particle correlation function. Underlying colored histogram represents the “mesh” obtained in the fitting procedure. The lines represent a fitted 2D parabola. The point represents the minimum of the parabola - the best fit value.

not possible to analyze them separately. In identical particle femtoscopy obtaining Gaussian source size parameters is straightforward: the integral in Eq. (15) can be performed analytically if one assumes that $S(\mathbf{r})$ is a 3D Gaussian and does not depend on pair momentum \mathbf{K} (although the pairs transverse momentum K_T dependence can be recovered by K_T binning; the rapidity binning is also possible). To take into account the Coulomb interaction, an approximate wave-function is used in which the Coulomb part is factorized out and replaced by an averaged function that only depends on the magnitude of k^* . This procedure [84], enables to write a simple analytic formula, which can be directly fitted to the 3D correlation function and provides femtoscopic radii.

In non-identical particle femtoscopy the Coulomb interaction is the source of the correlation, so it cannot be factorized out. Performing the integral in Eq. (15) analytically becomes impossible, especially when one needs to consider the strong interaction as well. The procedure must be carried out numerically. One starts with the same assumption as for identical particle femtoscopy. The source is a 3D Gaussian (33), where the additional modification allowing for a non-zero shift in the “out” direction is introduced. One then assumes a certain set of source parameters (R_{out} , R_{side} , R_{long} , μ_{out}) and calculates the corresponding correlation function, according to Eq. (15) and using the corresponding wave function (16). As the source function is assumed to be momentum independent, one needs an input momentum distribution (the assumption of momentum independence of the source function is not required provided the selected (p_T, y) is sufficiently narrow). This can be achieved by e.g. taking particles’ momenta from real pairs from data and assigning the separation \mathbf{r}^* randomly generated from (33). The resulting “model” CF is compared to the “measured” one via a χ^2 test. The procedure is repeated for several sets of source parameters to find the one that fits the “data” best. This set is taken as the result of the fit. The procedure can be refined by ensuring that the

“model” calculation is done for points which form a regular “mesh” in parameters’ space. In the simplest one parameter fit, one obtains the fit value and error from the location of χ^2 minimum on the parabola. When 2 independent parameters are fitted (the most common case for non-identical correlations, when we usually fit overall radius R and emission asymmetry μ) one creates a 2D “mesh”, to which one can fit a 2D parabola - obtaining the best fit parameters, their errorbars as well as the covariance between them. An example of such analysis is shown in Fig. 16. One can also employ a minimization package (e.g. Minuit) to perform the fitting process. The number of points in the CF “mesh” can be kept at minimum by using a simple linear or quadratic interpolation between points [10, 35].

For the results presented in this work we used a software package **CorrFit** to perform the numerical fitting procedure described above. It was developed for the analysis of non-identical particle correlations in the STAR experiment [39, 85]. It allows for significant flexibility when choosing various parameters of the fitting process. For this work we have made the following choices: (1) The input data were correlation functions in spherical harmonics representation. Only C_0^0 and $\mathcal{R}C_1^1$ components were fitted; the covariance between the two was taken into account. (2) The particular form of the S from Eq. (33) was taken with the additional constraints that R_{side} was assumed to be equal to R_{out} , while $R_{long} = 1.3R_{out}$, following the identical particle 3D femtoscopic results for pions from RHIC [86]. Therefore, only two independent parameters were fitted: R_{out} and μ_{out} . (3) The input momentum distributions were taken from the STAR experiment, ensuring that the momentum acceptance was the same. (4) The standard package from R. Lednický was used to calculate the pair weights [10, 14]. The input theoretical correlation functions were calculated taking into account Coulomb interaction only. In such case only the Coulomb part of the pair weight was calculated in the fitting procedure. (5) One had the possibility to introduce “pair purity” and momentum resolution corrections. Details of the purity correction will be discussed later in this Section. The momentum resolution correction was not necessary for model studies shown in this paper.

C. Influence of pair purity

For femtoscopic analysis one of the main experimental issues is the “purity” P of the analyzed pair sample, that is the fraction of pairs in the sample that should be treated as “femtoscopically correlated”. There are several reasons why a pair of particles should not be treated as correlated. From the experimental side, it may happen that one (or both) of the particles in the pair has been misidentified (this is why P is traditionally called “purity”). Another common scenario is when one of the particles is a product of a weak decay. In that case, it is the “parent” particle that should be treated

as “femtoscopically correlated”, leading in some cases to rather complicated cases of “residual correlations”, that is feed-down of femtoscopic correlation between parent particles into the daughters’ correlation function. Recently, such cases have been studied in detail in baryon–baryon correlations [41, 87]. However, in systems considered in this paper, containing a meson, residual correlations are smeared away by the decay momenta, so such pairs should be treated as “not femtoscopically correlated”. These experimental components of P are clearly experiment-dependent and it is up to the experiment to correct for such effects (or at least provide a realistic estimate of P). We will not address it further in this work.

However, another contribution to P remains, the estimate of which is model dependent. If one of the particles in the pair comes from a strongly decaying resonances that lives very long, e.g. the ω meson, we may need to treat it as “not femtoscopically correlated”. That is because the source of the correlation, the pair wave function Ψ is usually peaked at low r^* values, while at large values it produces no correlation. This can be dealt with in two ways. First is to assume, in the data analysis, a source function that perfectly describes such long-range r^* tails. However, this is difficult to do, and it is very dependent on the model that we use to model such tails. Another solution is to treat the particles in the tails as “not femtoscopically correlated” – in other words to provide a model estimate of the decrease of P coming from long-lived resonances. This is usually done by assuming that a source is a 3D sphere with a Gaussian profile, and counting any pair which is outside this sphere as non-correlated. We note that the “non-gaussian effects” have been seen in all RHIC experiments in the identical particle correlations [86, 88]. They have been attributed, at least in part, to long-lived resonances [53], and recently, new techniques have been proposed to analyze them in detail [89]. Such analysis are not yet possible in non-identical particle analysis, so we limit ourselves to the simple model estimation of P .

We characterize the overall “purity” of a pair sample by a percentage of pure pairs P . It can be (and in the experiment it usually is) a function of \mathbf{k}^* . Assuming that the “non-pure” pairs are not correlated, the correlation function can be trivially corrected for purity:

$$C_{corrected}(\mathbf{k}^*) = (C_{measured}(\mathbf{k}^*) - 1)/P(\mathbf{k}^*) + 1. \quad (36)$$

Employing the formula (36) requires a precise knowledge of the fraction of correlated pairs P in the measured sample. Any uncertainty in its value will be a source of the systematic error. In contrast to the identical particle femtoscopy, P cannot be easily inferred from the fit, independently of the source parameters σ and μ . By inspecting Fig. 10 and Eq. (36) one concludes that lowering purity influences the correlation function in a way that is similar to the changes introduced by varying the source size. One can obtain a satisfactory fit to the correlation function by adjusting either one of these parameters, so treating them both as free makes them highly correlated.

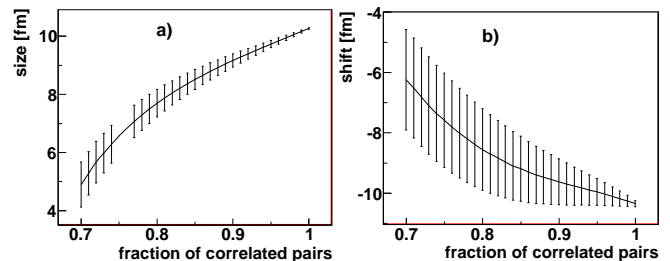


FIG. 17: Values of the correlation function fit (size a) and shift b)), as a function of a pre-defined fraction of primary pairs.

While possible, the independent determination of σ and P requires significant statistics and very good control of the non-femtoscopic background [10, 35].

Usually, the practical solution is to come up with the best estimate of P by other means (both experimental and theoretical), and fix its value for the fitting. By performing the procedure for several fixed values of P , within the reasonable uncertainty range, one obtains the systematic error on the fit values coming from the purity estimate. As an example on Fig. 17 we show how the fit values for the same input correlation function change as one adjusts the fixed pair purity P . Within the reasonable range of P variations of the order of 20% the dependence of σ and μ on P is monotonic and noticeable. We expect that the purity estimate will be the major source of the systematic error. We will address the theoretical part of the estimates of pair purity in Section VI B.

D. Influence of the momentum resolution

Momentum resolution will influence the femtoscopic correlation function in a well defined way. Since reconstructed momenta will differ from the true ones, the correlation effect (visible as either a “peak” or a “depression” at low k^*) will be reduced. The Coulomb correlation is rather sharp at low relative momentum, so one expects the small k^* points to be influenced the most. The “double-ratio” will be affected as well. One can study the influence of the momentum resolution by performing a theoretical calculation in the following way. One calculates C according to (32), but calculates two sets of relative momenta k^* for each pair. The first one k_{true}^* is used to calculate Ψ , the second one $k_{smeared}^*$ is used to determine the correlation function bin in which the pair is stored. The second set is calculated by smearing the particles’ momenta with the parametrization of the momentum resolution obtained from the experiment. By comparing the “unsmeared” and “smeared” correlation functions one can judge the importance of the momentum resolution effect. One can also employ the same technique when calculating the “theoretical” correlation functions during the fitting procedure described in Section V B. In this way the fitting procedure automatically corrects for momentum resolution. The precise determi-

nation of the momentum resolution parameters is very dependent on the experimental features. We will not discuss it further in this work (see, e.g. [35]).

VI. SYSTEMATIC CHECKS OF THE METHOD

In the previous sections we have made qualitative claims that the analysis of the non-identical particle correlations should enable the estimation of the source size and emission asymmetry for pions, kaons and protons emitted in the heavy-ion collision. In this section we aim to show the quantitative checks of the method. We focus on answering two questions: Can the method reliably and quantitatively recover the source size and emission asymmetry? If yes, what systematic uncertainties in this estimation come from the method itself?

We emphasize that in this Section we focus only on the technical aspect of the non-identical particle correlations method. So, the **THERMINATOR** calculations are used only as “test samples”.

A. Details of the procedure

We chose the following procedure: we simulate heavy-ion Au+Au collisions with the **THERMINATOR** model. We do it for 6 centrality bins: 0-5%, 5-10%, 10-20%, 20-30%, 30-40% and 40-50%. We calculate the full set of non-identical correlation functions: same and opposite sign pion-kaon, same and opposite-sign pion-proton and same sign kaon-proton for these centralities, producing $6 \times 5 = 30$ independent correlation functions. Then, we proceed to treat these functions as if they were experimental ones: applying the purity correction and fitting them with the **CorrFit** software. In the end we compare the input values from the model with the fit results and see if they match.

We simulated 50K events for each centrality. The parameters of the model were the same as the ones used in [26, 50], which are known to reproduce both single particle spectra and overall femtoscopic sizes from identical particle correlations. The correlation functions were calculated by combining particles from these events into pairs and employing Eq. (32). Spherical harmonics representation of the CF was used. Then, each function was fitted with the **CorrFit** program, assuming that the two-particle source is a 3D Gaussian in LCMS, according to Eq. (33). The sideward and longitudinal sizes of the source were fixed to be equal to R_{out} and $1.3R_{out}$ respectively, according to the results obtained for identical pions. In this way the fitting procedure had only two parameters: overall size R_{out} and emission asymmetry μ_{out} . We note that while the full 3D analysis, with R_{side} and R_{long} as independent free parameters of the fit, is in principle possible, we do not discuss it in this paper, as we consider it less interesting: it would provide 3D information about the source, but with much lower precision

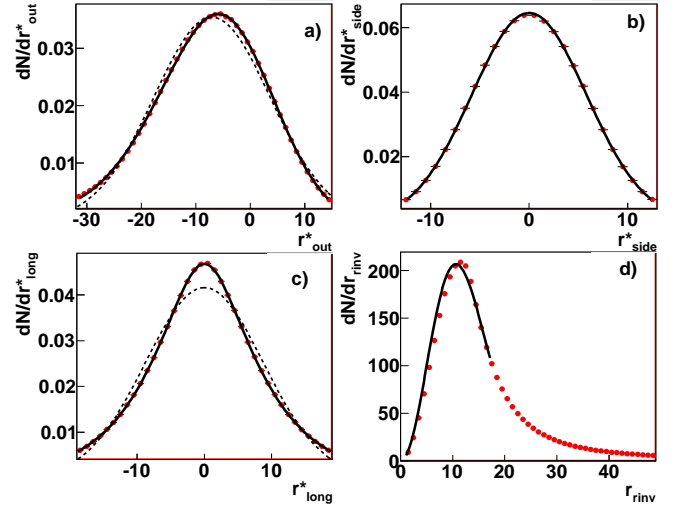


FIG. 18: Two-particle emission function for pion-kaon pairs at centrality 10-20%. r_{out}^* in a), r_{side}^* in b), r_{long}^* in c), r_{inv}^* in d). Lines are fits to the distributions, see text for details.

than the 3D identical pion analysis. Instead, we chose to focus on asymmetry, which is a unique observable accessible only via non-identical particle femtoscopy.

B. Characterizing model input

Let us inspect a typical two-particle emission function S_{AB} coming from the **THERMINATOR** model, shown in Fig. 18. The distributions in *out*, *side* and *long* directions show different behavior. Only the *side* one is well described by a Gaussian; attempts to fit the *out* and *long* by Gaussians are shown as dashed lines. The *long* can be described by an exponential hyperbola function:

$$f_{EH} = \exp \left(-\sqrt{\frac{r_{long}^{*2}}{\sigma_{long}^2} + \alpha^2} \right), \quad (37)$$

where σ and α are parameters. For the description of the *out* one needs an asymmetric exponential hyperbola:

$$f_{EH}^{as} = \exp \left(-\sqrt{\frac{(r_{out}^* - \mu_{out})^2}{\sigma_{out}^2} + \alpha^2} \right) (1 + \zeta(r_{out}^* - \mu_{out})), \quad (38)$$

where σ_{out} , μ_{out} , α_{out} and ζ are parameters. We have confirmed that these functional forms are general, that is, one is able to fit them to the emission functions at all centralities and for all pair types. In contrast, the fitting procedure that we have just described in the previous Section assumes a proper Gaussian source distribution. Therefore, one needs to find a suitable variable which will enable the comparison between the model input, which is non-Gaussian, with the fit output, which is postulated to be a Gaussian. In principle, one can think of removing the Gaussian assumption and actually using the functional forms mentioned above for the fitting.

This is certainly possible, both from the point of view of the technique as well as the software tools. However, it brings two potential problems. First of all, while the functional forms are able to fit the THERMINATOR data very well, there is no reason to assume it will be the case for other models. So, by choosing these particular forms one would introduce a strong model dependence. Moreover, it is not known how the parameters of these functions could be compared to the Gaussian radii from identical particle femtoscopy. In this work we access the overall directionally-averaged size of the system only, so the details of the source function dependence in the three directions separately will be lost. In this work we decided to use the Gaussian assumption, having in mind that it may introduce systematic effects, when comparing the fit values to input two-particle distributions.

We are then presented with the following situation: the “experimental” fit procedure produces the direction-averaged source size R and the emission asymmetry in *out* direction μ_{out} . On the other hand, to fully describe the theoretical model input, one needs the following parameters: σ_{out} , α_{out} , ζ , μ_{out} , σ_{side} , σ_{long} and α_{long} . To compare the two, one needs to find common variables which can be compared, and which will tell whether our “experimental fit” reproduces the “model input”.

In traditional HBT one compares 1-dimensional femtosopic radii, defined as a σ of a 1D-Gaussian approximation of the single-particle emission function (usually in PRF). We wish to define an analogous variable for non-identical study, but defined in LCMS to facilitate the comparisons to the 3D identical particle interferometry results. The task is complicated by the fact, that neither the “model input” nor the “experimental fit” produce a source which is a perfect Gaussian. Nevertheless, one can plot the source distribution dN/dr in both cases. Then, one fits the distribution with the Gaussian formula, multiplied by the proper Jacobian:

$$F_G(r) \approx \exp\left(-\frac{r^2}{2R_{av}^L}\right)r^2. \quad (39)$$

As will be discussed later, one must restrict the range of this fit to the low- r values, as these are the ones that contribute to the femtosopic effect. The contributions from the large- r part of the source must be dealt with separately. The lower-right part of Fig. 18 shows the example of the model r_{inv} distribution; the line is a fit according to (39), done in the range 0–20 fm. Since both r_{out} and r_{long} distributions are manifestly non-Gaussian, so is the r_{inv} distribution⁴. Therefore, the fitted R_{av}^{input} is only characterizing the general size of the system. The same fitting procedure can be applied to the r_{inv} distribution produced by the “experimental fit”, producing

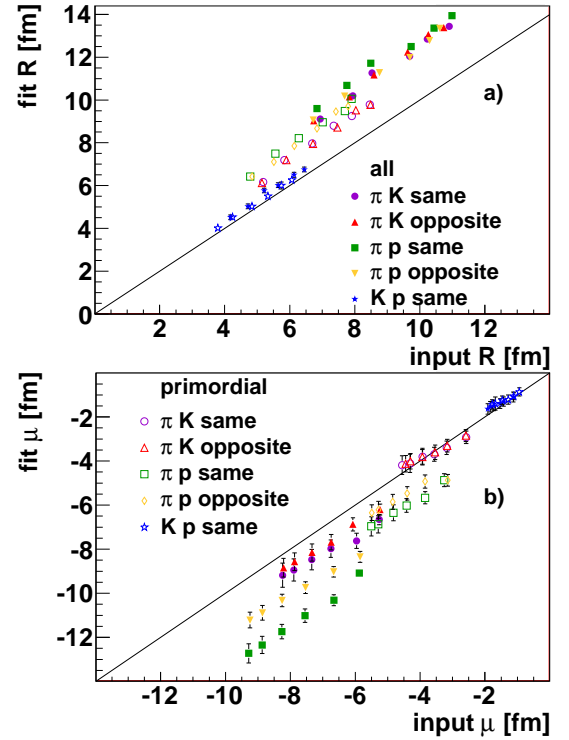


FIG. 19: (Color on-line) The correlation between input values obtained from model and fit values. Panel a) shows overall system size, b) - emission asymmetry in the *out* direction. Open points show calculations for primary particles only, closed points - for all particles. Violet circles are same-sign pion-kaon, red up-triangle: opposite-sign pion-kaon, green squares: same-sign pion-proton, yellow down-triangles: opposite-sign pion-proton, blue stars: same-sign kaon-proton.

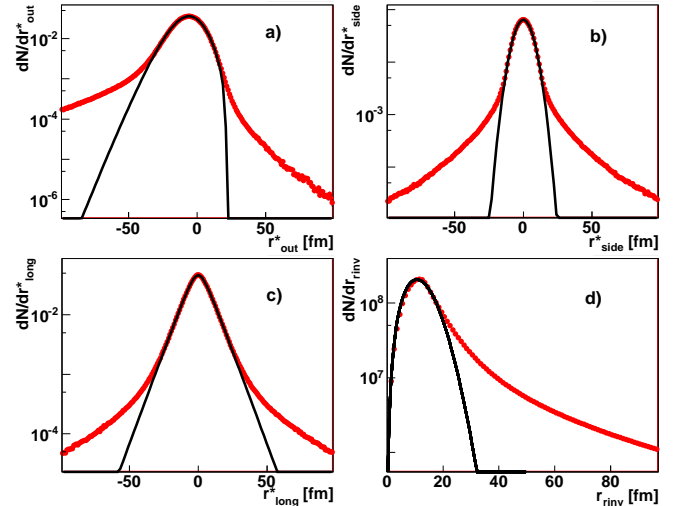


FIG. 20: An illustration of the long-range tails produced by THERMINATOR. Points: separation distributions for pion-kaon pairs, a): r_{out} , b): r_{side} , c): r_{long} , d) r_{inv} . Lines are fits to the region near the peak, using the functional forms: f_{EH}^{as} for *out*, Gaussian for *side*, f_{EH} for *long* and f_G for *inv*.

⁴ It can be shown that r_{inv} distribution is a Gaussian only if all three r_{out} , r_{side} and r_{long} are Gaussians and additionally all three have the same width.

the R_{av}^{fit} “experimental” value. For a more detailed dis-

TABLE V: Estimate of the theoretical purity P for all pair types, versus centrality. See text for details.

c [%]	0-5	5-10	10-20	20-30	30-40	40-50
πK	0.83	0.82	0.80	0.76	0.73	0.70
πp	0.80	0.79	0.77	0.75	0.73	0.71
$K p$	0.96	0.95	0.95	0.94	0.93	0.93

cussion of the approximate relations between 1D and 3D source size parameters, the relations between values in PRF and LCMS as well as a more detailed description of estimating R_{av} we refer the reader to Appendix A.

One also needs to define, what does “emission asymmetry” μ_{out} mean in the case of the model. One can come up with several definitions: (a) the “mean” of the r_{out}^* distribution, (b) the “mean” of the r_{out}^* distribution, but only taking into account parts of the distribution near to the peak (neglecting the long-range tail), (c) the position of the maximum in the r_{out}^* distribution. All three are correlated, but (a) shows large sensitivity to long-range tails and therefore is not well defined. Out of the other two (b) should be exactly the same as $\langle r_{out}^* \rangle$, which is the value used in the theoretical formalism, while the relation of (c) to $\langle r_{out}^* \rangle$ is less straightforward. So, we chose to use the definition (b).

In Fig. 19 the comparison between “input” and “fitted” radii is shown, for all considered pairs, both for primordial and all particles. A clear correlation is seen between the two. However, most of the results do not lie on the “perfect” $x = y$ line. Within each pair system the correlation is clear and monotonic. Moreover, the deviations from the “perfect” curve seem to be a systematic shift, similar for all points of the same pair type. The shift from perfect values for a given pair type is seen both for the R_{inv} and the μ_{out} variables.

One obvious candidate for the explanation of this shift is pair purity P . The fit procedure assumes that *all* the pairs in the source come from the region with Gaussian density profile. On the other hand, a realistic model, such as THERMINATOR, clearly shows that there are significant non-Gaussian long-range tails in the separation distributions; this is illustrated in Fig. 20. One can perform a simple calculation. Take the model radius R_{av}^L obtained from fitting the model separation distribution with (39) and by integrating this distribution one obtains the number of pairs N_G within the Gaussian core of the source. N_G is then the area below the fit curve on the lower-right panel of Fig. 20. This can be compared to the total number of pairs N_A obtained by simply counting the number of model pairs, or in other words - the area below the points on the lower-right panel of Fig. 20. The value $f_{FC} = N_G/N_A$ is the number of “femtoscopically correlated” pairs and should be simply treated as “purity” in the sense discussed in Section V C. One needs to correct for these “non-gaussian” effects. In order to do that one calculates f_{FC} and then treats it as a fixed parameter in the fitting process. Note that the f_{FC} estimation

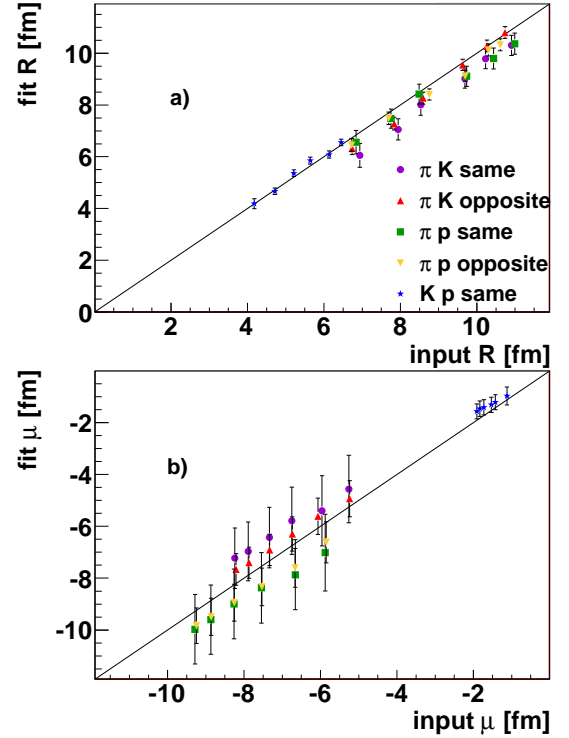


FIG. 21: (Color on-line) Same as Fig. 19, but the fit procedure is done with adjusted purity values (see text for details).

procedure by design takes into account two effects, which cannot be easily disentangled - the pairs in the long-range tails and the fact that the shape of the core system is not a Gaussian in a 1D representation. We have performed the estimation, based on the input model pair separation distributions and find that f_{FC} depends both on the pair type and centrality. The exact values are given in Tab. V. These values are obviously model dependent and are strongly influenced by the size of the long-range tails in the separation distributions. It is well known that the source of such tails are, to a large degree, particles coming from the strongly decaying resonances. It is therefore important to use a model like THERMINATOR, which fully includes all known resonance propagation and decay, to determine purity. A clear trend exists for all pair types: the f_{FC} get smaller as collisions get more peripheral. The long-range resonance tails and non-Gaussian effects get relatively more important as one moves away from central collisions.

The “experimental fits” have been redone, this time with “purity” fixed to the listed f_{FC} values. The results are shown in Fig. 21. All results now lie close to the “perfect” $x = y$ line within the statistical error. This shows that, having in mind the caveat mentioned above, the analysis technique is able to produce reliable results, and that the results of the “experimental fitting” procedure do indeed provide a valuable information about the particle-emitting source. In particular, both the direction-averaged size of the source and the emission asymmetry can be reliably recovered.

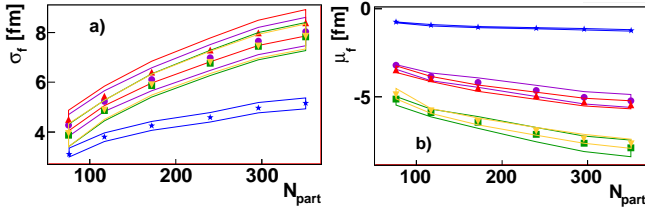


FIG. 22: (Color on-line) Fitted parameters for all pair types, versus centrality. System size (σ) in panel a), emission asymmetry (μ) in b). Colors and symbols are the same as in Fig. 19. The bands represent the change in the fit parameters as the fixed purity P is changed by ± 0.05 for pion-kaon and pion-proton pairs and ± 0.03 for kaon-proton.

The inherent uncertainty in the determination of f_{FC} is the source of the systematic error introduced by the method itself. In Fig. 22 we show how the fit value changes when purity is varied within a reasonable range (± 0.05 for pion-kaon and pion-proton and ± 0.03 for kaon-proton). This results in the following systematic uncertainties on the obtained values: for same-sign pion-kaon 7% on σ and 7% on μ , for opposite-sign pion-kaon 7% on σ and 4% on μ , for same-sign pion-proton 8% on σ and 6% on μ , for opposite-sign pion-proton 7% on σ and 4% on μ , for same-sign kaon-proton 5% on σ and 4% on μ .

We note that the f_{FC} estimation presented here is specific to THERMINATOR and represents the uncertainty within this model itself. In addition, the absolute value as well as an estimated uncertainty of f_{FC} can be different in other models, e.g. in rescattering codes. The total systematic uncertainty of the experimental measurement should take this model dependence into account. In addition, the experimental “purity”, that is the efficiency of particle identification, will also contribute to the same uncertainty.

VII. RESULTS OF “EXPERIMENTAL-LIKE” ANALYSIS

In Section V we have described, in detail, the experimental procedure to analyze the non-identical particle correlations. For the model analysis of the THERMINATOR output, we have used the complete two-particle method for calculating the correlation function and we have obtained the pion-kaon, pion-proton and kaon-proton correlation functions. They are, from a point of view of a formalism and our analysis methods, identical to the correlation functions that one might obtain in the experiment. We calculated sets of 1D histograms which correspond to these functions represented in spherical harmonics. We neglected the strong interaction component of the pair wave-function for simplicity and speed of calculation. Then we switched this effect off in the fitting procedure as well. Obviously, when fitting the true experimental functions, one will use the full pair wave-function calculation. The strong interaction effect

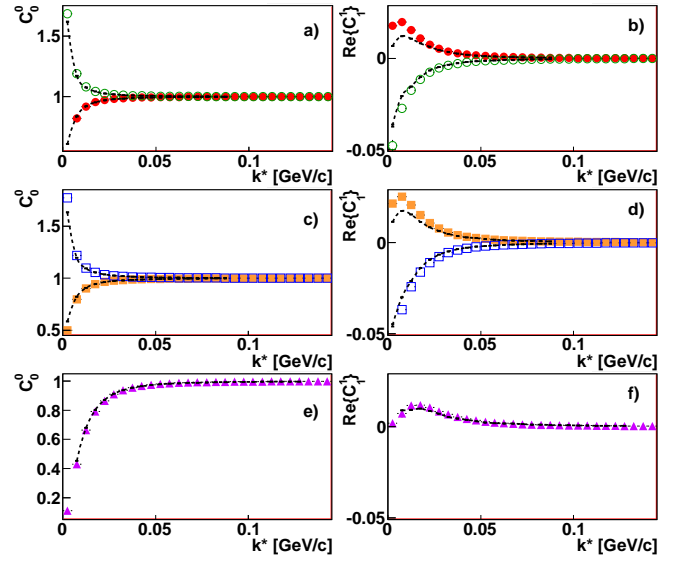


FIG. 23: (Color on-line) Example of the correlation functions calculated from THERMINATOR+Lhyquid model for central Au+Au collisions. Panels a), c), e) show the C_0^0 components, panels b), d), f) show $\Re C_1^1$. Closed circles are same-sign pion-kaon, open circles opposite-sign pion-kaon, closed squares are same-sign pion-proton, open squares are opposite-sign pion-proton, triangles are same-sign kaon-proton. Lines show the best-fit “model” correlation functions.

is known to be small compared to the Coulomb for the pairs of interest, so we do not expect any systematic effect on the fit values coming from this simplification. In addition, in the real experimental correlation function, one expects some non-femtoscopic effects in addition to the pure femtoscopic one. These need to be dealt with on a case-by-case basis, as they will strongly depend on experimental conditions. For this discussion we assume that any such effects can be identified and that the experimental correlation function can be properly corrected, so that only the femtoscopic effect remains.

We proceeded to treat the calculated correlation functions as if they were coming from the experiment. No other information, except of the pair purities is used in the procedure. For purity correction we used values listed in Tab. V, as we would have done in the real data analysis. The goal of the exercise is to confirm that the obtained “experimental fit values” actually correspond to the true values, shown in the previous Section and obtained directly from the emission functions. The example correlation functions together with the fitted “model” ones are shown in Fig. 23. For pion-kaon and pion-proton one can see the positive correlation effect for opposite-sign pairs and a negative one for same-sign pairs. The $\Re C_1^1$ components also show mirror effect. For kaon-proton the correlation effects start at larger k^* (is wider) and is more pronounced, as expected from a smaller Bohr radius for this pair. The lines show the functions fitted with the CorrFit program.

The fitting described in Sec. IV assumes that the source is a 3D Gaussian in LCMS. The direct output

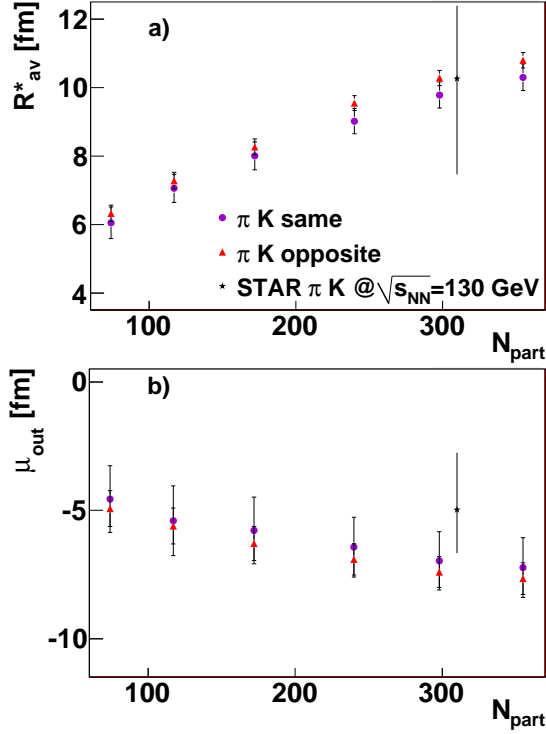


FIG. 24: (Color on-line) The source parameters in PRF for pion-kaon pairs obtained from the “experimental” fitting procedure. Panel a) shows source size, b): emission asymmetry. Circles show same-sign pairs, triangles: opposite sign. Open star is a STAR measurement [39] at $\sqrt{s_{NN}} = 130$ GeV, the line represents statistical+systematic error (see text for details).

of the fitting procedure is a size of the system in the *out* direction σ_f and the emission asymmetry μ_f in that direction. From these values one can calculate, via the relations specified in Appendix A, all the other source size characteristics. In the fitting procedure each pair is treated individually, so its velocity is known. One can therefore directly determine the direction averaged source size in PRF - there is no need to use averaged pair velocity in transformation from LCMS to PRF, like in Eq. (A15). In Figs. 24, 25, 26 we plot this directionally averaged radii in PRF R_{av}^* . Out of the three equivalent values: σ_f , R_{av}^L and R_{av}^* one must choose one for presentation of the results. When we present the results of our calculations, we chose R_{av}^* , as it is more natural than σ_f (which requires the knowledge of other directions multipliers in order to be meaningful) and describes the emission function in PRF, so there is no need for assumptions required in the LCMS to PRF transformation. On the other hand, the 3D identical particle femtoscopy analysis produces source sizes directly in LCMS, so if we want to compare to these results, we will use R_{av}^L .

In Fig. 24 we show the “experimental-like” fit results R_{av}^* for pion-kaon pairs. This should be compared to the “true” values from Fig. 6. The correlation between “true” and “fitted” values is also shown directly in

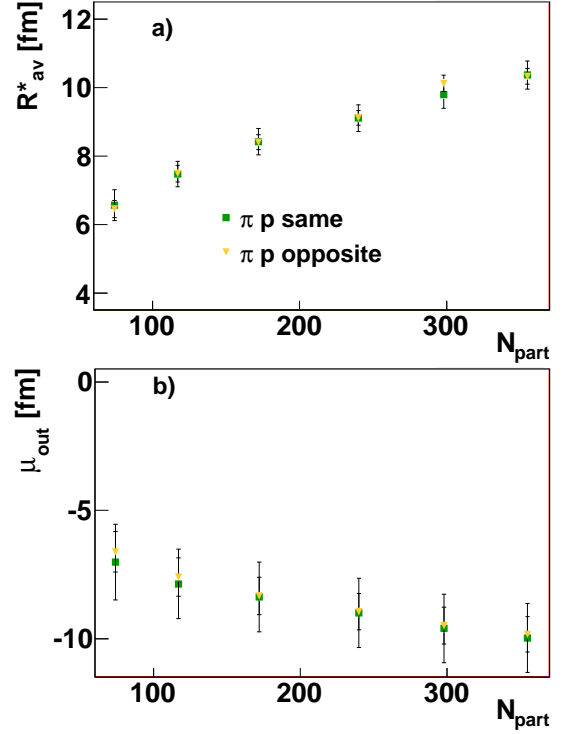


FIG. 25: (Color on-line) The source parameters in PRF for pion-proton pairs obtained from the “experimental” fitting procedure. Panel a): source size, b): emission asymmetry. Squares show same-sign pairs, triangles: opposite sign.

Fig. 21. We can see that even with all the assumptions and simplifications that are used in the fitting procedure one is able to recover the true system size. The accuracy for same-sign pion-kaon function is 8%, for opposite-sign is 5%, with the largest deviation of 10%. These are comparable to the statistical error of the fit. For the asymmetry the “input” and “fit” values were identical within 10%. All results were in agreement within statistical error of the fit.

A single measurement is available for the pion-kaon system at RHIC, done by STAR at $\sqrt{s_{NN}} = 130$ GeV [39]. To compare it with the values presented in Fig. 24 we needed to account for two effects. The measurement was corrected for a fraction of *non-primary* particles (particles not coming from the primary vertex), which is an experimental correction. But, it was not corrected for *non-correlated primary pairs*, a correction which we described in this work. Taking the dependency in Fig. 17 as a guideline and the purity estimate of 0.85 for pion-kaon in central Au+Au we have scaled the reported system size and asymmetry accordingly. Moreover, the fitting performed in [39] assumed a specific shape (size equal in *out*, *side* and *long* directions in PRF), from which we recalculated R_{av}^* , to be compared with results in this work. The measurement was done at a colliding energy different than the one considered in this work, so we plot the result at a corresponding N_{part} . One can see that the system size is in perfect

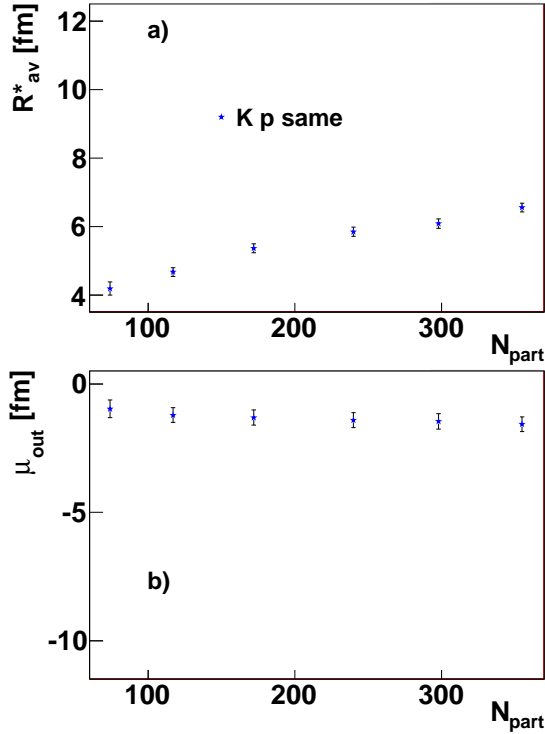


FIG. 26: (Color on-line) The source parameters in PRF for kaon–proton pairs obtained from the “experimental” fitting procedure. Panel a) shows source size, b): emission asymmetry.

agreement with the model predictions in this work; the asymmetry seems to be slightly smaller than the prediction, but in agreement within statistical+systematic error.

In Fig. 25 the same results are shown for pion–proton pairs. The accuracy of the system size determination is 5%, comparable to the statistical fit error. The asymmetry is reproduced with worse quality, with discrepancies of up to 12%, comparable to the statistical error.

In Fig. 26 the results are shown for kaon–proton pairs. The system size determination is good: 3%, better than the statistical fit error. The asymmetry is reproduced with discrepancies of up to 15%; however, since the absolute values are small (compared to the pion–kaon and pion–proton case), the absolute value of the difference is comparable with the systematic error of the fit. We conclude that the system size and the emission asymmetry can be reliably recovered, with the systematic error due to the procedure itself less than 10%. However, one must correctly determine the systematic error due to the pair purity estimation as well. We note that the tests of the method have been performed for Therminator model only, so they are not necessarily general. However the tests were done for many centralities (system sizes) and pair types and the method was found to be working in all cases, so we have some confidence that it should work for other models as well. One possibility for further studies would be to perform similar tests with a model that

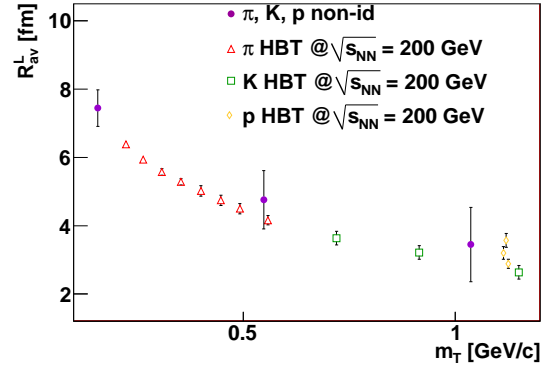


FIG. 27: (Color on-line) Comparison of overall size obtained from the non-identical particle calculation with the RHIC data for central Au+Au collisions at 200 GeV/c. Closed circles are (from left to right) single particle pion, kaon and proton radii inferred from non-id simulations (centrality 5-10%); open triangles are pion radii from STAR [90] (centrality 0-5%), open squares are pion radii from PHENIX [91] (centrality 0-30%), open diamonds are proton results from STAR [87] (centrality 0-10%).

introduces particle rescatterings.

One would also like to compare the results of non-identical particle correlations with the wealth of data coming from femtoscopic analysis at RHIC. This presents a complication, since the identical-particle femtoscopy is usually presented in 3D form as single particle “HBT radii” R_{out} , R_{side} and R_{long} , while for analysis in this work we only have averaged two-particle source size σ^f and emission asymmetry μ_{out}^f . From its definition we conclude that e.g. $\sigma_{\pi K}^f$ should correspond to the variance of convolution of two Gaussians: one with variance of R_{out} for pions and the other with variance of R_{out} for kaons at the same velocity. Both the identical particle R ’s and the non-identical σ^f are defined in LCMS. Again we refer the reader to Appendix A for explicit relations between the two. From the input data (either R_{out} , R_{side} and R_{long} in LCMS for identical particles or σ_f and μ_f for non-identical) we calculate the directionally averaged source size R_{av}^L . By comparing these values, defined in LCMS, as opposed to the R_{inv} defined in PRF, we avoid the unnecessary approximation coming from the determination of the averaged pair velocity, needed for the determination of $\langle \gamma \rangle$. Such comparison is made in Fig. 27, where data from most central Au+Au collisions are shown. The open points are experimental data for pions, kaons and protons. The closed points are single-particle source sizes inferred from fits to the non-identical particle correlation functions calculated for THERMINATOR. One can see a very good agreement between the model prediction and the data. All datapoints follow the “ m_T scaling” trend predicted by hydrodynamics. A direct comparison of non-identical particle sizes and asymmetries between model and data would be an even better test. However we stress that such comparisons can only be made, provided that other observables

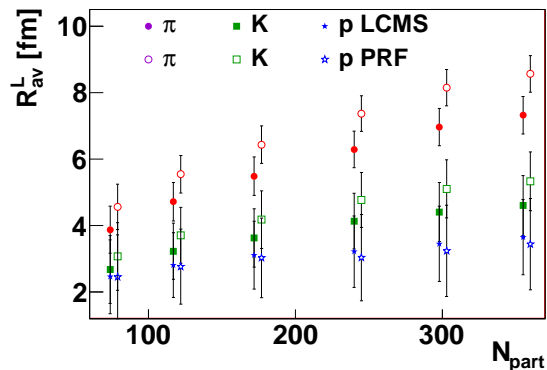


FIG. 28: (Color on-line) The single-particle source sizes inferred from the non-identical simulations versus centrality. Closed points are for LCMS sizes, open (shifted for clarity) for PRF. Circles are pions, squares: kaons, stars: protons.

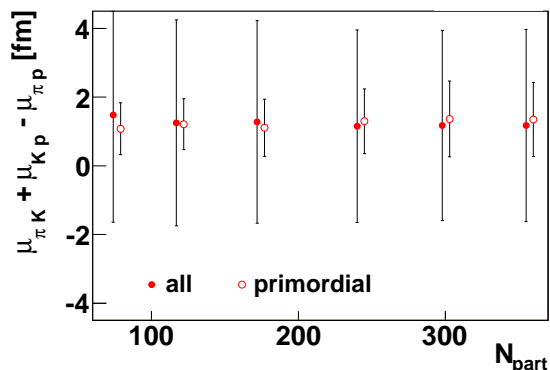


FIG. 29: (Color on-line) Emission asymmetry consistency cross-check versus centrality. Closed points are for all particles, open (shifted for clarity) for primordial only.

related to source dynamics, such as e.g. particle spectra, elliptic flow and identical particle femtoscopy are reproduced in the model. These tests have been performed for *Therminator* in earlier works [26, 50].

We have calculated the single-particle source sizes for all centralities and plotted them in Fig. 28. An ordering of source sizes with particle mass is seen as expected, as well as increase of the overall source size with N_{part} . Sizes for PRF are larger, as the *out* radius is scaled by the $\langle \gamma_t \rangle$ factor.

As a final cross-check we show in Fig. 29 that the emission asymmetries do add up to zero within the systematic error of the measurement.

VIII. CONCLUSIONS

The *THERMINATOR*+Lhyquid model was briefly introduced, and shown to have a unique set of features: hydrodynamic expansion and inclusion of resonance propagation and decay for all known particle types. Both features are important for non-identical particle femtoscopy. Simulations with this model provided predictions for emission asymmetries between particles of different masses,

and validated the analysis methods of non-identical particle femtoscopy.

We underlined the importance of the emission asymmetry measurement and provided predictions for RHIC energies. We showed that “emission asymmetry”, or the non-zero difference in the mean emission points of particles of same velocity but different mass is predicted to arise in hydrodynamical calculation. It was shown to be intimately related to the collective behavior of matter and to be a direct consequence of the $x-p$ correlations. It is the most direct and unambiguous femtoscopic signal of such behavior, and provides an independent strong constraint on the models aiming to describe the space-time evolution of the heavy-ion collision. Specific predictions, both qualitative and quantitative, have been given for such asymmetries, for all the considered pair types (pion-kaon, pion-proton, kaon-proton). It was shown that the lighter particle is always emitted closer to the center of the source, giving a negative emission asymmetry μ_{out} in the *out* direction. Predictions for the size of the source, including the dependence on centrality, were also given, which were cross-checked with the more precise results from identical particle femtoscopy.

The influence of strongly decaying resonances on emission asymmetries was also studied in detail. It was shown that due to a specific combination of decay kinematics’ properties for particles of different masses, the emission asymmetry produced by an earlier hydrodynamic stage is further magnified. At the same time the resonance decay process alone produces emission asymmetry an order of magnitude smaller than the $x-p$ correlation, so it cannot be used as an alternative explanation of the phenomenon.

We have presented, in some detail, the theoretical basis and some technical aspects of the non-identical particle femtoscopy, to be used in ultra-relativistic heavy-ion collisions. In particular it was shown how to access the “emission asymmetry”, a piece of femtoscopic information that can only be accessed via this type of analysis. It was pointed out that spherical harmonics representation of the correlation function has useful synergies with the analysis; the use of such representation was strongly advocated. Important corrections to the correlation function were identified: pair purity and momentum resolution, and experimentalist recipes were given for applying them to the real data. Extracting femtoscopic information from the non-identical particle correlation function requires a numerical fitting procedure. It was described in detail, and implemented as a computer code. It was also shown that, after application of the proper purity correction, the fit procedure was able to recover the “true” model input values, which was an important validation of the method.

An estimate of the “fraction of correlated pairs”, coming from significant non-Gaussian shape and long-range tails in the pair separation distributions, has been obtained, based on the *THERMINATOR* simulation. The value can be an input to an experimental analysis of RHIC data, however one must keep in mind that it is model

dependent. The systematic error coming from this theoretical estimate was also given.

Finally, the “experimentalists” analysis procedure, described in the paper, was applied to the correlation functions obtained from the model calculations. It was shown that the method reliably recovers the input model values in realistic conditions. Internal consistency cross-checks were proposed and tested. The way to compare results of non-identical particle femtoscopy and the femtoscopic sizes from identical particle analysis was presented; the THERMINATOR predictions were shown to be in agreement with available identical particle HBT radii results from RHIC.

Acknowledgements

I would like to thank Richard Lednicky, Wojciech Florkowski and Yiota Foka for comments and very helpful discussions.

Appendix A: Emission function measures

In femtoscopy one considers pairs of particles. Of particular interest are observables related to their relative separation \mathbf{r} . We refer the reader to the beginning of Section III for the description of symbol conventions, the reference system and the relevant reference frames. The transition from LCMS to PRF is simply the boost along the outwards direction, with the transverse velocity of the pair β_t :

$$\begin{aligned} r_{out}^* &= \gamma_t (r_{out} - \beta_t \Delta t) \\ r_{side}^* &= r_{side} \\ r_{long}^* &= r_{long} \\ \Delta t^* &= \gamma_t (\Delta t - \beta_t r_{out}). \end{aligned} \quad (A1)$$

However, in our calculation we always use the equal time approximation, which means that we neglect the time difference Δt^* in the PRF. From the components we also calculate the length of the relative separation vector:

$$r^* \equiv r_{inv} = \sqrt{r_{out}^{*2} + r_{side}^{*2} + r_{long}^{*2}}. \quad (A2)$$

The two-particle emission function is, from a mathematical point of view, any function of the separation four-vector, $S(\Delta x)$, where $\Delta x = \{\Delta t, \mathbf{r}\}$ can be expressed in any reference frame. In femtoscopy we use specific functional forms of S , which are characterized by parameters. One must keep in mind that even though the relation between *relative separation* \mathbf{r} values in LCMS and PRF is given by simple equation Eq. (A1), the relations between *source function parameters* (R ’s and μ) in these reference frames may not be so simple. Moreover, even if there exists a simple parametrization of the source in 3D variables

$(r_{out}, r_{side}, r_{long})$, it does not mean that this source distribution expressed in the magnitude of the relative separation r will also have a simple parametric form. The aim of this Appendix is to derive relations between commonly used source function parameters, defined in various reference frames as well as between 3D and 1D representation parameters. Similar considerations, for different source parametrizations have been done in the past [92].

We must also repeat the description of Eq. (21) where we state that the two-particle emission function S_{AB} is (in case of independent emission) a convolution of two single particle emission functions. Let us emphasize this complication of the femtoscopic measurement: we are interested in the *single particle* emission functions, as they directly characterize the source. On the other hand femtoscopy provides information about the *two-particle* (or *relative*) emission functions only. Moreover, the convolution procedure of Eq. (21) is not reversible. It means that, in a strict mathematical sense, one cannot recover the full information about the individual single particle emission functions by measuring only the separation distribution. Nevertheless, in femtoscopic measurements, reasonable additional assumptions can be made and we are able to recover some of the information. In this Appendix we will discuss how to extract the single-particle emission function parameters from the measured two-particle ones.

1. Traditional emission function parametrizations

We list here the traditional functional forms of the emission function that are used in femtoscopy and list their parameters. The easiest is the 1-dimensional “ R_{inv} ” parametrization:

$$\begin{aligned} S_{1d}^P(\mathbf{r}^*) &\equiv \frac{dN}{d^3\mathbf{r}} = \exp\left(-\frac{r_{out}^{*2} + r_{side}^{*2} + r_{long}^{*2}}{4R_{inv}^2}\right) \\ S_{1d}^P(r^*) &\equiv \frac{dN}{dr^*} = r^{*2} \exp\left(-\frac{r^{*2}}{4R_{inv}^2}\right). \end{aligned} \quad (A3)$$

Note that the formulas neglect the Δt^* dependence, which is possible thanks to the equal-time approximation in PRF, allowing one to neglect Δt^* dependence of $|\Psi|^2$. The change from the 3D variables to the 1D one requires the introduction of the proper Jacobian. Let us also explain the factor of 4 before the “Gaussian sigma” R_{inv} instead of the usual 2. It is a particular property of a Gaussian distribution that a convolution of two Gaussians is also a Gaussian with its sigma being the quadratic sum of the sigmas of the individual distributions. The R_{inv} parametrization is used for identical particles, for which Eq. (21) can be simplified by noticing that both emission functions are the same. If one assumes that a single-particle emission function is a Gaussian, then the two-particle one is also a Gaussian with σ multiplied by $\sqrt{2}$. Therefore, by fitting the *two-particle* distribution with the functional form (A3) one conveniently obtains the *single-particle* σ : the R_{inv} . Therefore, the

R_{inv} “HBT radii” reported by experiments are the single-particle emission function Gaussian widths, where the emission function is assumed to be a 3D Gaussian in the PRF.

A more sophisticated emission function form, used by all RHIC and SPS experiments to report identical pion femtoscopy results is:

$$S_{3d}^L(\mathbf{r}) = \exp\left(-\frac{r_{out}^2}{4R_{out}^L} - \frac{r_{side}^2}{4R_{side}^L} - \frac{r_{long}^2}{4R_{long}^L}\right). \quad (A4)$$

We again note the factor of 4 before the σ 's, making them the single-particle widths. The important difference is that this emission function has three independent width R_{out}^L , R_{side}^L and R_{long}^L and they are defined in the LCMS (hence the L superscript), not in PRF. Note that, unlike in PRF, we do not use equal-time approximation in LCMS. For identical particles this is not a problem: only the Coulomb part of the wave-function depends on Δt , but it is factorized out in the usual fitting procedures, and replaced by the averaged value. For non-identical particles one can adopt one of two approaches. One can continue to use Eq. (A5) to be consistent with identical particle femtoscopy, but in this case the Δt spread will get absorbed into the three spatial radii. Or one can add the fourth component with the time spread to Eq. (A5). Since we aim to compare the results from non-identical and identical particle analysis and since we are in any case only able to recover the dimensionally-averaged source size for non-identical particles we chose the first solution.

For non-identical particles we must make one additional modification, the mean emission point should be allowed to differ from zero, at least in the *out* direction. Moreover the simple connection between the single- and two-particle sizes is no longer possible, since the underlying single-particle emission functions are now different:

$$S_{3d}^{L,N}(\mathbf{r}) = \exp\left(-\frac{(r_{out} - \mu_{out}^L)^2}{2R_{out}^L} - \frac{r_{side}^2}{2R_{side}^L} - \frac{r_{long}^2}{2R_{long}^L}\right). \quad (A5)$$

We introduced an additional parameter: the mean of the distribution in the *out* direction μ_{out}^L and the source sizes are now the *two-particle* ones.

In order to facilitate the comparison between 1D and 3D source sizes in LCMS we also introduce the emission function with one, directionally averaged, source size in LCMS R_{av}^L :

$$S_{1d}^{L,N}(\mathbf{r}) = \exp\left(-\frac{(r_{out} - \mu_{out}^L)^2 + r_{side}^2 + r_{long}^2}{2R_{av}^L}\right). \quad (A6)$$

2. Relating 1D and 3D source sizes

The non-identical particle femtoscopy has been, so far, limited to the measurement of the directionally averaged

source size R_{av}^L . A question arises, what is the relation between R_{av}^L and three-dimensional source sizes R_{out} , R_{side} and R_{long} . Let us write explicitly the form of the emission function in magnitude of r :

$$S_{3d}^L(r) = \int \exp\left(-\frac{r_{out}^2}{2R_{out}^L} - \frac{r_{side}^2}{2R_{side}^L} - \frac{r_{long}^2}{2R_{long}^L}\right) \times \delta(r - \sqrt{r_{out}^2 + r_{side}^2 + r_{long}^2}) dr_{out} dr_{side} dr_{long}. \quad (A7)$$

To find the 1D source size corresponding to the 3 3D ones, we assume that the above distribution can be approximated by:

$$S_{1d}^L(r) = r^2 \exp\left(-\frac{r^2}{2R_{av}^L}\right). \quad (A8)$$

First, let us note that S_{3d}^L simplifies exactly to S_{1d}^L only in the special case of $R_{out}^L = R_{side}^L = R_{long}^L$, in which case $R_{av}^L = R_{out}^L$. If this condition is not met, the S_{3d}^L is *not* a Gaussian in r , and the exact mathematical relation between the 1D and 3D sizes does not exist. Nevertheless, for realistic values of radii, S_{3d}^L is not very different from a Gaussian and can be well approximated by S_{1d}^L . One can find an effective approximate relation between R_{av}^L and $(R_{out}^L, R_{side}^L, R_{long}^L)$ numerically in the following way. One generates a significant sample of triplets $(r_{out}, r_{side}, r_{long})$ where r_{out} is randomly generated from a Gaussian of width R_{out}^L , r_{side} with width R_{side}^L etc. Then, one constructs a distribution $S(\sqrt{r_{out}^2 + r_{side}^2 + r_{long}^2})$, to which one then fits numerically the functional form (A8). The results of the fit, R_{av}^L is the approximate 1D source size that we seek. We may also want to restrict the fit range to small values of r in order to minimize the dependence on non-Gaussian features which will mostly affect the large- r region. We have performed such calculations and concluded that the approximate relation is:

$$R_{av}^L = \sqrt{(R_{out}^L)^2 + R_{side}^L{}^2 + R_{long}^L{}^2}/3. \quad (A9)$$

Note that the pair velocity does not enter into the derivation, so it is equally valid for LCMS and PRF.

In addition, in non-identical particle femtoscopy one is able to access the first moments of the source distribution. Then, S has the general form of: $S(R_{out}^L, R_{side}^L, R_{long}^L, \mu_{out}^L, \mu_{side}^L, \mu_{long}^L)$. Due to symmetry relations μ_{side}^L must vanish. For collider experiments with symmetric rapidity acceptance μ_{long}^L vanishes as well, which leaves one additional parameter μ_{out}^L . By performing a numerical procedure very similar to the one in the previous paragraph (the only difference being that the r_{out} is now randomly generated from a Gaussian with the mean of μ_{out}^L) we obtained an equivalent approximate

effective relation:

$$R_{av}^L = \sqrt{(R_{out}^L{}^2 + R_{side}^L{}^2 + R_{long}^L{}^2)/3 + 0.3\mu_{out}^L{}^2}. \quad (A10)$$

3. Relating single-particle and two-particle sizes

As already mentioned for identical particles the relation between two-particle and single particle sizes is a trivial $\sqrt{2}$ factor if the assumption of a Gaussian emission function is made. For non-identical particle sizes such simple connection is not possible, and even an approximate one can only be made after certain simplifications are done. Let us assume that the two particle types, A and B are emitted according to the emission functions S_A and S_B which are Gaussians. The two particle emission function is then:

$$\begin{aligned} S_{AB}(\mathbf{r}) = & \int \exp \left(-\frac{(x_{out}^A - \mu_{out}^A)^2}{2R_{out}^A{}^2} - \frac{x_{side}^A{}^2}{2R_{side}^A{}^2} - \frac{x_{long}^A{}^2}{2R_{long}^A{}^2} \right) \\ & \times \exp \left(-\frac{(x_{out}^B - \mu_{out}^B)^2}{2R_{out}^B{}^2} - \frac{x_{side}^B{}^2}{2R_{side}^B{}^2} - \frac{x_{long}^B{}^2}{2R_{long}^B{}^2} \right) \\ & \times \delta(r_{out} - x_{out}^A + x_{out}^B) dx_{out}^A dx_{out}^B \\ & \times \delta(r_{side} - x_{side}^A + x_{side}^B) dx_{side}^A dx_{side}^B \\ & \times \delta(r_{long} - x_{long}^A + x_{long}^B) dx_{long}^A dx_{long}^B. \end{aligned} \quad (A11)$$

Performing the integration and neglecting the unimportant normalization constants one obtains:

$$\begin{aligned} S_{AB} = & \exp \left(-\frac{[r_{out} - (\mu_{out}^A - \mu_{out}^B)]^2}{2(R_{out}^A{}^2 + R_{out}^B{}^2)} \right) \\ & \times \exp \left(-\frac{r_{side}^2}{2(R_{side}^A{}^2 + R_{side}^B{}^2)} \right) \\ & \times \exp \left(-\frac{r_{long}^2}{2(R_{long}^A{}^2 + R_{long}^B{}^2)} \right) \end{aligned} \quad (A12)$$

giving us immediately $\mu_{out}^{AB} = \mu_{out}^A - \mu_{out}^B$ and $R_x^{AB} = \sqrt{R_x^A{}^2 + R_x^B{}^2}$, as expected. Obviously, one cannot recover the two single-particle source sizes from the one two-particle size. However, in this work we have calculated three independent two-particle sizes: for pion-kaon, pion-proton and kaon-proton systems. Therefore we have a set of three equations (A12), with A and B being π and K in the first one, π and p in the second one and K and p in the third one respectively. This set of equations has three unknowns, the single particle source sizes: R^π , R^K and R^p , so we can solve it to calculate them.

The procedure has to be carried out in a few steps. We start with the fit values σ_f . From this we calculate the approximate overall averaged source size R_f^{av} , following our fit assumptions: $R_{out} = \sigma_f$, $R_{side} = \sigma_f$ and $R_{long} =$

$1.3\sigma_f$. With these values we write the set of equations for the particle source sizes:

$$\begin{aligned} \sigma_f^{\pi K} &= \sqrt{\sigma_f^{\pi 2} + \sigma_f^{K 2}} \\ \sigma_f^{\pi p} &= \sqrt{\sigma_f^{\pi 2} + \sigma_f^{p 2}} \\ \sigma_f^{Kp} &= \sqrt{\sigma_f^{K 2} + \sigma_f^{p 2}} \end{aligned} \quad (A13)$$

and solve it obtaining:

$$\begin{aligned} \sigma_f^\pi &= \sqrt{(\sigma_f^{\pi K 2} + \sigma_f^{\pi p 2} - \sigma_f^{Kp 2})/2} \\ \sigma_f^K &= \sqrt{(\sigma_f^{\pi K 2} - \sigma_f^{\pi p 2} + \sigma_f^{Kp 2})/2} \\ \sigma_f^p &= \sqrt{(-\sigma_f^{\pi K 2} + \sigma_f^{\pi p 2} + \sigma_f^{Kp 2})/2}. \end{aligned} \quad (A14)$$

From these fit parameters one then calculates directionally averaged single-particle radius R_{av}^L with Eq. (A9) - σ_f is treated as R_{out}^L . These can be compared to the R_{av}^L directionally averaged radii in LCMS, which can be calculated with Eq. (A9) from the *single-particle* 3D HBT radii published by the RHIC experiments.

4. Dealing with non-Gaussian source functions

Let us now consider a non-Gaussian source, as it is evident, e.g. from this work, that realistic models predict that the emitting source will not have a perfect Gaussian shape. However, the two-particle emission function, defined as a convolution of two single-particle sources, is required to be closer to Gaussian than the single-particle functions. And the single particle functions themselves, even though non-Gaussian, are not very different: they usually have a large peak and some long-range tails. From this we conclude that even though we know that the two-particle source function is not Gaussian, we may assume that it will have Gaussian-like features: it will have a peak, and the distribution around that peak can be reasonably approximated by a Gaussian. It will also usually have long-range non-Gaussian tails. This means that we can define two variables that can be used as measures of the variance: either the RMS of the distribution, or the σ of a Gaussian fit to the peak structure in the emission function. For the study of non-identical particle averaged sizes σ is the proper variable to be used. That is because pair wave functions, which are the source of femtoscopic correlation, contain strong structures near zero r^* , while at large r^* they do not produce any correlation. On the other hand the RMS of the distribution will be very sensitive to the long-range tails, which is undesirable in our case. Therefore we define that a “femtoscopic size” R for a non-Gaussian emission function is simply the σ of a Gaussian fitted to the two-particle emission function near its peak.

5. Obtaining R_{av} from models

In models we know the emission function exactly. Therefore we can infer R_{av} directly from it. We do this numerically, in a manner very similar to the one shown in previous sections. First we determine the probability distributions for various components of r : $f_o(r_{out})$, $f_s(r_{side})$, $f_l(r_{long})$. For the THERMINATOR calculation, discussed in this work, we have found that f_o has the form of (38), f_s is Gaussian, and f_l has the form (37). Now we proceed with the generation of triplets, construction of the $S(r)$ and numerical fitting to obtain R_{av} . Such R_{av} can then be directly compared to the R_{av} obtained from the “experimental” fitting procedure described above.

6. Relations between source sizes in LCMS and PRF

We can write approximate relations between source sizes in the two reference systems, they are:

$$\begin{aligned} R_{out}^* &= R_{out} \langle \gamma_t \rangle \\ R_{side}^* &= R_{side} \\ R_{long}^* &= R_{long} \\ \mu_{out} &= \langle \gamma_t \rangle \mu_{out}^L \end{aligned} \quad (A15)$$

Using Eqs. (A9), (A10) one can obtain the relations for the averaged 1D radius R_{av}^* as well. One must also independently determine the $\langle \gamma_t \rangle$ for the pair sample used in a given analysis.

-
- [1] G. I. Kopylov and M. I. Podgoretsky, Sov. J. Nucl. Phys. **15**, 219 (1972).
 - [2] G. I. Kopylov and M. I. Podgoretsky, Sov. J. Nucl. Phys. **18**, 336 (1974).
 - [3] G. Goldhaber, S. Goldhaber, W.-Y. Lee, and A. Pais, Phys. Rev. **120**, 300 (1960).
 - [4] R. Hanbury Brown and R. Q. Twiss, Phil. Mag. **45**, 663 (1954).
 - [5] R. H. Brown and R. Q. Twiss, Nature **177**, 27 (1956).
 - [6] R. Hanbury Brown and R. Q. Twiss, Nature **178**, 1046 (1956).
 - [7] R. Lednicky, V. L. Lyuboshits, B. Erasmus, and D. Nouais, Phys. Lett. **B373**, 30 (1996).
 - [8] S. Voloshin, R. Lednicky, S. Panitkin, and N. Xu, Phys. Rev. Lett. **79**, 4766 (1997), nucl-th/9708044.
 - [9] R. Lednicky, S. Panitkin, and N. Xu (2003), nucl-th/0304062.
 - [10] R. Lednicky, Phys. Part. Nuclei **40**, 307 (2009), nucl-th/0501065.
 - [11] S. Pratt, Braz. J. Phys. **37**, 871 (2007), nucl-th/0612006.
 - [12] R. Lednicky and V. L. Lyuboshits, Sov. J. Nucl. Phys. **35**, 770 (1982).
 - [13] D. H. Boal, C. K. Gelbke, and B. K. Jennings, Rev. Mod. Phys. **62**, 553 (1990).
 - [14] R. Lednicky, Journal of Physics G: Nuclear and Particle Physics **35**, 125109 (27pp) (2008), URL <http://stacks.iop.org/0954-3899/35/125109>.
 - [15] B. e. a. Erasmus, Proc. CORINNE II, Nantes, France, 6-10 Sept. 1994, Ed. J. Aichelin and D. Ardouin, World Scientific pp. 116–128 (1994), SUBATECH 94-17, Nantes.
 - [16] R. Kotte et al. (FOPI), Eur. Phys. J. **A6**, 185 (1999), nucl-ex/9904007.
 - [17] D. Gourio et al. (INDRA), Eur. Phys. J. **A7**, 245 (2000), nucl-ex/0001004.
 - [18] R. Ghesi et al., Phys. Rev. Lett. **87**, 102701 (2001), nucl-ex/0108017.
 - [19] J. Helgesson, R. Ghesi, and J. Ekman, Phys. Rev. **C73**, 044602 (2006), nucl-ex/0509028.
 - [20] J. Adams et al. (STAR), Nucl. Phys. **A757**, 102 (2005), nucl-ex/0501009.
 - [21] K. Adcox et al. (PHENIX), Nucl. Phys. **A757**, 184 (2005), nucl-ex/0410003.
 - [22] U. W. Heinz and P. F. Kolb (2002), hep-ph/0204061.
 - [23] T. Hirano, Acta Phys. Polon. **B36**, 187 (2005), nucl-th/0410017.
 - [24] M. A. Lisa, S. Pratt, R. Soltz, and U. Wiedemann, Ann. Rev. Nucl. Part. Sci. **55**, 357 (2005), nucl-ex/0505014.
 - [25] P. Huovinen and P. V. Ruuskanen, Ann. Rev. Nucl. Part. Sci. **56**, 163 (2006), nucl-th/0605008.
 - [26] W. Broniowski, M. Chojnacki, W. Florkowski, and A. Kisiel, Phys. Rev. Lett. **101**, 022301 (2008), 0801.4361.
 - [27] Y. M. Sinyukov, Acta Phys. Polon. **B37**, 3343 (2006).
 - [28] Y. M. Sinyukov, A. N. Nazarenko, and I. A. Karpenko, Acta Phys. Polon. **B40**, 1109 (2009), 0901.3922.
 - [29] S. Pratt, Acta Phys. Polon. **B40**, 1249 (2009), 0812.4714.
 - [30] S. Pratt and J. Vredevoogd, Phys. Rev. **C78**, 054906 (2008), 0809.0516.
 - [31] S. A. Voloshin, A. M. Poskanzer, and R. Snellings (2008), 0809.2949.
 - [32] P. Sorensen (2009), 0905.0174.
 - [33] S. V. Akkelin and Y. M. Sinyukov, Phys. Lett. **B356**, 525 (1995).
 - [34] C. Gombeaud, T. Lappi, and J.-Y. Ollitrault (2009), 0901.4908.
 - [35] R. Lednicky, NA49 Note number **210** (1999), 0112011.
 - [36] C. Blume et al., Nucl. Phys. **A715**, 55 (2003), nucl-ex/0208020.
 - [37] D. Antonczyk and D. Miskowiec, Braz. J. Phys. **37**, 979 (2007), hep-ph/0702219.
 - [38] D. Miskowiec (1998), nucl-ex/9808003.
 - [39] J. Adams et al. (STAR), Phys. Rev. Lett. **91**, 262302

- (2003), nucl-ex/0307025.
- [40] P. Chaloupka (STAR) (2007), 0705.3480.
 - [41] J. Adams et al. (STAR), Phys. Rev. **C74**, 064906 (2006), nucl-ex/0511003.
 - [42] F. Retiere and M. A. Lisa, Phys. Rev. **C70**, 044907 (2004), nucl-th/0312024.
 - [43] U. W. Heinz and P. F. Kolb, Nucl. Phys. **A702**, 269 (2002), hep-ph/0111075.
 - [44] T. Hirano, K. Morita, S. Muroya, and C. Nonaka, Phys. Rev. **C65**, 061902 (2002), nucl-th/0110009.
 - [45] T. Hirano and K. Tsuda, Nucl. Phys. **A715**, 821 (2003), nucl-th/0208068.
 - [46] D. Zschesche, S. Schramm, H. Stoecker, and W. Greiner, Phys. Rev. **C65**, 064902 (2002), nucl-th/0107037.
 - [47] J. Socolowski, O., F. Grassi, Y. Hama, and T. Kodama, Phys. Rev. Lett. **93**, 182301 (2004), hep-ph/0405181.
 - [48] A. Kisiel, T. Taluc, W. Broniowski, and W. Florkowski, Comput. Phys. Commun. **174**, 669 (2006), nucl-th/0504047.
 - [49] G. Torrieri et al., Comput. Phys. Commun. **167**, 229 (2005), nucl-th/0404083.
 - [50] A. Kisiel, W. Broniowski, M. Chojnacki, and W. Florkowski, Phys. Rev. **C79**, 014902 (2009), 0808.3363.
 - [51] M. Chojnacki and W. Florkowski, Phys. Rev. **C74**, 034905 (2006), nucl-th/0603065.
 - [52] M. Chojnacki and W. Florkowski, Acta Phys. Polon. **B38**, 3249 (2007), nucl-th/0702030.
 - [53] A. Kisiel, W. Florkowski, and W. Broniowski, Phys. Rev. **C73**, 064902 (2006), nucl-th/0602039.
 - [54] W. Broniowski, M. Rybczynski, and P. Bozek (2007), arXiv:0710.5731 [nucl-th].
 - [55] R. Andrade, F. Grassi, Y. Hama, T. Kodama, and J. Socolowski, O., Phys. Rev. Lett. **97**, 202302 (2006), nucl-th/0608067.
 - [56] Y. Hama et al. (2007), 0711.4544.
 - [57] D. Kharzeev and M. Nardi, Phys. Lett. **B507**, 121 (2001), nucl-th/0012025.
 - [58] A. Bialas, M. Bleszynski, and W. Czyz, Nucl. Phys. **B111**, 461 (1976).
 - [59] B. B. Back et al. (PHOBOS), Phys. Rev. **C65**, 031901 (2002), nucl-ex/0105011.
 - [60] B. B. Back et al. (PHOBOS), Phys. Rev. **C70**, 021902 (2004), nucl-ex/0405027.
 - [61] W. M. Yao et al. (Particle Data Group), J. Phys. **G33**, 1 (2006).
 - [62] W. Broniowski, P. Bozek, and M. Rybczynski, Phys. Rev. **C76**, 054905 (2007), 0706.4266.
 - [63] Y. Aoki, Z. Fodor, S. D. Katz, and K. K. Szabo, JHEP **01**, 089 (2006), hep-lat/0510084.
 - [64] P. Braun-Munzinger, D. Magestro, K. Redlich, and J. Stachel, Phys. Lett. **B518**, 41 (2001), hep-ph/0105229.
 - [65] W. Broniowski and W. Florkowski, Phys. Rev. Lett. **87**, 272302 (2001), nucl-th/0106050.
 - [66] W. Broniowski and W. Florkowski, Phys. Rev. **C65**, 064905 (2002), nucl-th/0112043.
 - [67] J. Rafelski, J. Letessier, and G. Torrieri, Phys. Rev. **C72**, 024905 (2005), nucl-th/0412072.
 - [68] D. Prorok (2007), nucl-th/0702042.
 - [69] F. Cooper and G. Frye, Phys. Rev. **D10**, 186 (1974).
 - [70] D. Teaney, J. Lauret, and E. V. Shuryak, Phys. Rev. Lett. **86**, 4783 (2001), nucl-th/0011058.
 - [71] C. Nonaka and S. A. Bass, Phys. Rev. **C75**, 014902 (2007), nucl-th/0607018.
 - [72] T. Hirano, U. W. Heinz, D. Kharzeev, R. Lacey, and Y. Nara, J. Phys. **G34**, S879 (2007), nucl-th/0701075.
 - [73] N. S. Amelin et al., Phys. Rev. **C74**, 064901 (2006), nucl-th/0608057.
 - [74] R. Lednicky, Phys. Atom. Nucl. **67**, 73 (2004).
 - [75] R. Lednicky and T. B. Progulova, Z. Phys. **C55**, 295 (1992).
 - [76] A. Kisiel, Acta Phys. Pol. B **40**, 1155 (2009).
 - [77] R. Lednicky, Braz. J. Phys. **37**, 939 (2007), nucl-th/0702063.
 - [78] B. Borasoy, R. Nissler, and W. Weise, Eur. Phys. J. **A25**, 79 (2005), hep-ph/0505239.
 - [79] B. e. a. Erasmus (1998), SUBATECH 98-03, Nantes.
 - [80] R. Lednicky, Acta Phys. Pol. B **40**, 1145 (2009).
 - [81] P. Danielewicz and S. Pratt, Phys. Rev. **C75**, 034907 (2007), nucl-th/0612076.
 - [82] Z. Chajecki and M. Lisa, Phys. Rev. **C78**, 064903 (2008), 0803.0022.
 - [83] A. Kisiel and D. A. Brown (2009), 0901.3527.
 - [84] Y. Sinyukov, R. Lednicky, S. V. Akkelin, J. Pluta, and B. Erasmus, Phys. Lett. **B432**, 248 (1998).
 - [85] A. Kisiel, Nukleonika **49 (Supplement 2)**, S81 (2004).
 - [86] J. Adams et al. (STAR), Phys. Rev. **C71**, 044906 (2005), nucl-ex/0411036.
 - [87] H. P. Gos, Eur. Phys. J. **C49**, 75 (2007).
 - [88] S. S. Adler et al. (PHENIX), Phys. Rev. Lett. **93**, 152302 (2004), nucl-ex/0401003.
 - [89] S. S. Adler et al. (PHENIX), Phys. Rev. Lett. **98**, 132301 (2007), nucl-ex/0605032.
 - [90] S. Collaboration, Physical Review C **71**, 044906 (2005), URL doi:10.1103/PhysRevC.71.044906.
 - [91] . S. Afanasiev (PHENIX) (2009), 0903.4863.
 - [92] A. D. Chacon et al., Phys. Rev. **C43**, 2670 (1991).